Nuclear Structure from a Novel Beyond-Mean-Field Model

Towards Super-Heavy Nuclei from Densities and Mean-Fields to Wave Functions and Observables

Ljungberg, Jimmy

2024

Document Version:
Publisher's PDF, also known as Version of record

Nuclear Structure from a Novel Beyond-Mean-Field Model

Towards Super-Heavy Nuclei from Densities and Mean-Fields to Wave Functions and Observables

JIMMY LJUNGBERG
DEPARTMENT OF PHYSICS | FACULTY OF ENGINEERING | LUND UNIVERSITY

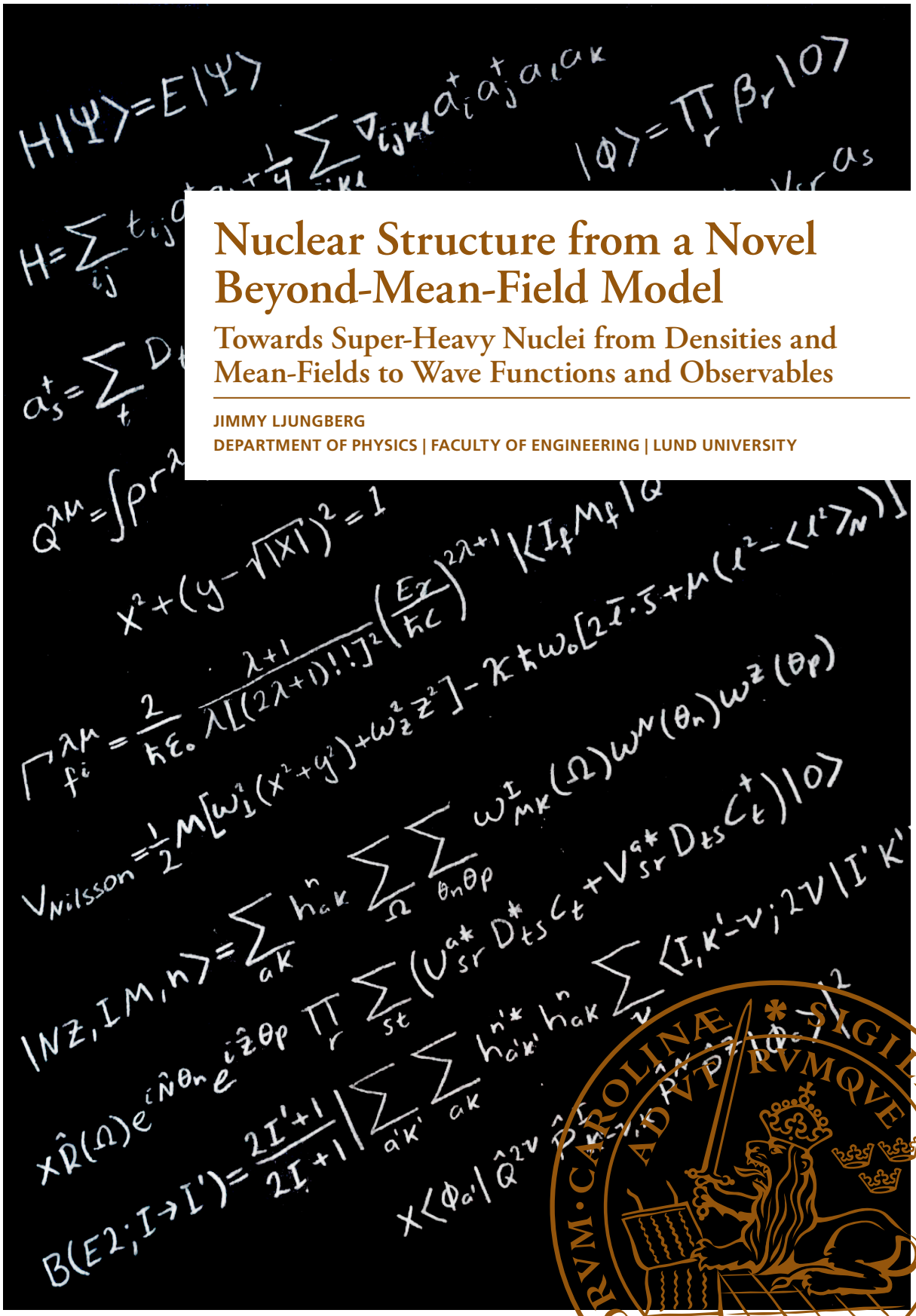

Nuclear Structure from a Novel Beyond-Mean-Field Model

Nuclear Structure from a Novel Beyond-Mean-Field Model

Towards Super-Heavy Nuclei from Densities and Mean-Fields to Wave Functions and Observables

Jimmy Ljungberg

LUND
UNIVERSITY

Thesis for the degree of Doctor of Philosophy
Thesis advisors: Gillis Carlsson and Andréa Idini
Faculty opponent: Markus Kortelainen

To be presented, with the permission of the Faculty of Engineering at Lund University, for public criticism in the Rydberg lecture hall (Rydbergsalen) at the Department of Physics on Friday, the 28th of November 2024 at 13:00.

Organization
LUND UNIVERSITY

Department of Physics
Division of Mathematical Physics
Box 118, SE–221 00 Lund
Sweden

Document name
DOCTORAL THESIS

Date of disputation
2024-11-28

Sponsoring organization

Author
Jimmy Ljungberg

Title
Nuclear Structure from a Novel Beyond-Mean-Field Model

Abstract
This thesis is dedicated to the construction of a novel model for nuclear structure; aimed at heavy and super-heavy nuclei. The model builds upon, and extends, nuclear density functional theory. The model describes a mapping of an energy density functional into an effective Hamiltonian which is postulated to have a simple form. This Hamiltonian is solved in the frameworks of the generator coordinate method and projections onto good quantum numbers. The outputs are energies and wave functions expressed in the laboratory system. The wave functions are further used to calculate electromagnetic moments and transition rates. Due to the simplicity of the Hamiltonian, the model can be used for super-heavy nuclei.

The first part of this thesis places the research of this work in a larger context. The constructed model is motivated and in detail described. As a demonstration for how the model is used, a calculation and the produced results for the nucleus ^{48}Cr are presented. The second part reproduces the papers for which this thesis is based upon.

Paper I study the α-decay $^{219}\mathrm{Ra} \rightarrow {}^{215}\mathrm{Rn}$ both experimentally and theoretically. The theoretical study investigates the octupole deformation and the α-decay rates of ^{219}Ra with nuclear density functional theory and its spectrum with the many-particle+rotor model.

Paper II presents experimental data for an α-decay chain of the man-made super-heavy elements ^{292}Lv, ^{288}Fl and ^{284}Cn. This chain runs through the anticipated shell gap at $Z = 114$. The paper also contains a theoretical study in which the model presented in this thesis is used to calculate the spectra for ^{282,284,286,288}Cn.

Paper III is the main work of this thesis. It describes the different parts of the model presented in this thesis in a thorough manner. How electromagnetic transition rates can be calculated within the model is shown. Results obtained from the model for ^{48,49,50,52}Cr and ^{24}Mg are presented.

Paper IV extends upon the model to include odd numbered angular momentum states. Three types of Skyrme parametrizations, UNEDF1, SLy4 and SkM*, are investigated.

Key words
nuclear structure, super-heavy nuclei, effective Hamiltonian, beyond-mean-field, temperature, good quantum numbers, spectra, wave functions, electromagnetic transition rates

Classification system and/or index terms (if any)

Supplementary bibliographical information

Language
English

ISSN and key title

ISBN
978-91-8104-135-4 (print)
978-91-8104-136-1 (pdf)

Recipient's notes

Number of pages
156

Price

Security classification

Nuclear Structure from a Novel Beyond-Mean-Field Model

Towards Super-Heavy Nuclei from Densities and Mean-Fields to Wave Functions and Observables

Jimmy Ljungberg

LUND
UNIVERSITY

A doctoral thesis at a university in Sweden takes either the form of a single, cohesive research study (monograph) or a summary of research papers (compilation thesis), which the doctoral student has written alone or together with one or several other author(s).

This is a compilation thesis and consists of two parts. An introductory framework puts the research work into context and describes in great depth the methodology behind the published papers. Then, the research publications themselves are reproduced, together with a description of the contributions made by the author of this thesis.

Cover illustration front: A selection of equations relevant for Nuclear Physics in general and for this Thesis in particular. Also, the unit Heart.

Cover illustration back: Alternative title in Swedish suggested by my middle son Love, age 7. It can be translated to "Tricky facts about Atomic nuclei". The picture is made by my eldest son Leo, age 9, and shows his interpretation of an atom. Beryllium I guess? My youngest son Tyko, age 3, has contributed by being our own little nucleus of the family.

Funding information: The thesis work was financially supported by the Knut and Alice Wallenberg Foundation (KAW 2015.0021).

Faculty of Engineering, Department of Physics, Division of Mathematical Physics

ISBN: 978-91-8104-135-4 (print)
ISBN: 978-91-8104-136-1 (pdf)

Printed in Sweden by Media-Tryck, Lund University, Lund 2024

Media-Tryck is a Nordic Swan Ecolabel certified provider of printed material. Read more about our environmental work at www.mediatryck.lu.se

MADE IN SWEDEN

All Children are Scientists
Some of us just don't grow up

The Book of Nature is written in the Language of Mathematics
— Galileo Galilei

Contents

List of publications i
Acknowledgements v
Popular Scientific Introduction and Summary vii

I Introductory Framework **1**

1 Introduction **3**
1.1 Nuclear History 4
1.2 Experimental Motivations for The Model 7

2 Nuclear Theory **11**
2.1 Theoretical Frameworks – An Overview 12
2.2 Established Theory used within The Model 16

3 Description of The Model **27**
3.1 Issues with an EDF in GCM and Projections 28
3.2 The Effective Hamiltonian 29
3.3 Mapping an EDF into The Effective Hamiltonian 36
3.4 The Many-Body Basis 38
3.5 Temperature 40
3.6 GCM and Projections 43
3.7 Solving the Hill-Wheeler Equation 44

4 Electromagnetic Transitions **47**
4.1 Electric Multipole Moments 48
4.2 The Reduced Transition Rate 49
4.3 Formalism within The Model 51

5 Computations and Results **53**
5.1 Computations for the Nucleus ^{48}Cr 54
5.2 Mean-Field – Single-Particle Quantities 54
5.3 Beyond-Mean-Field – Many-Body Quantities 55
5.4 Results 58

6 Outlook **61**

References **65**

A Structure of Computer Code **71**

B Discretization of Projection Operators **73**

C Matrix Elements in the Many-Body Basis **75**
C.1 The Effective Hamiltonian 75
C.2 The Quadrupole Operator 77

D The Transpose of the Quadrupole Matrix **79**

II Scientific Publications **81**

Author's Contributions **83**
Paper I: Low-lying states in ^{219}Ra and ^{215}Rn: Sampling microsecond α-decaying nuclei 85
Paper II: Spectroscopy along Flerovium Decay Chains: Discovery of ^{280}Ds and an Excited State in ^{282}Cn 99
Paper III: Nuclear spectra from low-energy interactions 109
Paper IV: Beyond-Mean-Field with an Effective Hamiltonian Mapped from an Energy Density Functional 127

List of publications

This thesis is based upon the following publications:

I **Low-lying states in ^{219}Ra and ^{215}Rn: Sampling microsecond α-decaying nuclei**

A. Såmark-Roth, L.G. Sarmiento, D. Rudolph, **J. Ljungberg**, B.G. Carlsson, C. Fahlander, U. Forsberg, P. Golubev, I. Ragnarsson, D. Ackermann, L.L. Andersson, M. Block, H. Brand, D.M. Cox, A. Di Nitto, Ch. E. Düllmann, K. Eberhardt, J. Even, J.M. Gates, J. Gerl, K.E. Gregorich, C.J. Gross, R.D. Herzberg, F.P. Heßberger, E. Jäger, J. Khuyagbaatar, B. Kindler, I. Kojouharov, J.V. Kratz, J. Krier, N. Kurz, B. Lommel, A. Mistry, C. Mokry, J.P. Omtvedt, P. Papadakis, J. Runke, K. Rykaczewski, M. Schädel, H. Schaffner, B. Schausten, P. Thörle-Pospiech, N. Trautmann, T. Torres, A. Türler, A. Ward, N. Wiehl, A. Yakushev

Physical Review C, **98**, 044307, (2018)

II **Spectroscopy along Flerovium Decay Chains: Discovery of ^{280}Ds and an Excited State in ^{282}Cn**

A. Såmark-Roth, D.M. Cox, D. Rudolph, L.G. Sarmiento, B.G. Carlsson, J.L. Egido, P. Golubev, J. Heery, A. Yakushev, S. Åberg, H.M. Albers, M. Albertsson, M. Block, H. Brand, T. Calverley, R. Cantemir, R.M. Clark, Ch. E. Düllmann, J. Eberth, C. Fahlander, U. Forsberg, J.M. Gates, F. Giacoppo, M. Götz, S. Götz, R.D. Herzberg, Y. Hrabar, E. Jäger, D. Judson, J. Khuyagbaatar, B. Kindler, I. Kojouharov, J.V. Kratz, J. Krier, N. Kurz, L. Lens, **J. Ljungberg**, B. Lommel, J. Louko, C.C. Meyer, A. Mistry, C. Mokry, P. Papadakis, E. Parr, J.L. Pore, I. Ragnarsson, J. Runke, M. Schädel, H. Schaffner, B. Schausten, D.A. Shaughnessy, P. Thörle-Pospiech, N. Trautmann, J. Uusitalo

Physical Review Letters, **126**, 032503, (2021)

III **Nuclear spectra from low-energy interactions**

J. Ljungberg, B.G. Carlsson, J. Rotureau, A. Idini, I. Ragnarsson

Physical Review C, **106**, 014314, (2022)

IV **Beyond-Mean-Field with an Effective Hamiltonian Mapped from an Energy Density Functional**

J. Ljungberg, J. Boström, B.G. Carlsson, A. Idini, J. Rotureau

Journal of Physics: Conference Series, **2586**, 012081, (2023)

Publications not included in this thesis:

1 **Towards microscopic optical potentials in deformed nuclei**

A. Idini, J. Rotureau, J. Boström, **J. Ljungberg**, B. G. Carlsson

Journal of Physics: Conference Series, **2586**, 012049, (2023)

2 **Spectroscopic factors with generator coordinate method and application to ^{25}Mg states**

J. Boström, J. Rotureau, **J. Ljungberg**, B. G. Carlsson, A. Idini

Journal of Physics: Conference Series, **2586**, 012080, (2023)

3 **Spectroscopy along flerovium decay chains. II. Fine structure in odd-A ^{289}Fl**

D.M. Cox, A. Såmark-Roth, D. Rudolph, L.G. Sarmiento, R.M. Clark, J.L. Egido, P. Golubev, J. Heery, A. Yakushev, S. Åberg, H.M. Albers, M. Albertsson, M. Block, H. Brand, T. Calverley, R. Cantemir, B.G. Carlsson, Ch.E. Düllmann, J. Eberth, C. Fahlander, U. Forsberg, J.M. Gates, F. Giacoppo, M. Götz, S. Götz, R.-D. Herzberg, Y. Hrabar, E. Jäger, D. Judson, J. Khuyagbaatar, B. Kindler, I. Kojouharov, J.V. Kratz, J. Krier, N. Kurz, L. Lens, **J. Ljungberg**, B. Lommel, J. Louko, C.-C. Meyer, A. Mistry, C. Mokry, P. Papadakis, E. Parr, J.L. Pore, I. Ragnarsson, J. Runke, M. Schädel, H. Schaffner, B. Schausten, D.A. Shaughnessy, P. Thörle-Pospiech, N. Trautmann, J. Uusitalo

Physical Review C, **107**, L021301, (2023)

4 **Spectroscopy along flerovium decay chains. III. Details on experiment, analysis, ^{282}Cn, and spontaneous fission branches**

A. Såmark-Roth, D.M. Cox, D. Rudolph, L.G. Sarmiento, M. Albertsson, B.G. Carlsson, J.L. Egido, P. Golubev, J. Heery, A. Yakushev, S. Åberg, H.M. Albers, M. Block, H. Brand, T. Calverley, R. Cantemir, R.M. Clark, Ch.E. Düllmann, J. Eberth, C. Fahlander, U. Forsberg, J.M. Gates, F. Giacoppo, M. Götz, S. Götz, R.-D. Herzberg, Y. Hrabar, E. Jäger, D. Judson, J. Khuyagbaatar, B. Kindler, I. Kojouharov, J.V. Kratz, J. Krier, N. Kurz, L. Lens, **J. Ljungberg**, B. Lommel, J. Louko, C.-C. Meyer, A. Mistry, C. Mokry, P. Papadakis, E. Parr, J.L. Pore, I. Ragnarsson, J. Runke, M. Schädel, H. Schaffner, B. Schausten, D.A. Shaughnessy, P. Thörle-Pospiech, N. Trautmann, J. Uusitalo

Physical Review C, **107**, 024301, (2023)

5 **Collective wavefunction of Yrast states in ^{50}Cr**

A. Idini, **J. Ljungberg**, J. Boström, B.G. Carlsson

Nuovo Cimento della Societa Italiana di Fisica C, **47**, 31 (2024)

Acknowledgements

I would like to express my deepest gratitude to my supervisor Gillis Carlsson who believed in me and gave me the opportunity to make my dream come true; my dream of doing research as a theoretical physicist. He has opened up the beautiful land of nuclear physics to me and has with great patience guided me through all of my work. Without him this thesis would never have happened.

Also, I am deeply grateful that I have been allowed to be on parental leave; whenever I wanted and how much I wanted. This has enabled me to spend time with my three boys when they are at an age when it perhaps means the most.

Many thanks to Andréa Idini who encouraged me to attend and give a speech at the International Nuclear Physics Conference 2022 in Cape Town, South Africa and guided me during the trip. This was the highlight of my PhD-studies. The combination of high level research communication with magnificent nature made the visit an experience for life.

Min älskade fru. Tack för att du har följt med mig på denna galna resa till Skåne; jag hade aldrig gjort det utan dig. Tack för att du har gett mig chansen att leva ut min dröm. Jag är dig evigt tacksam för ditt stöd och din kärlek.

Popular Scientific Introduction and Summary

This thesis is dedicated for the construction of a theoretical model for the description of atomic nuclei.

The Atomic Nucleus

Imagine the smallest thing that you could investigate with your bare senses. What size does it have? Maybe around 1 mm? With that size you can see its shape and feel it with your fingers.

Of course, for smaller objects we can use a microscope to see them. But when we enter the world of atoms, which are roughly of the size 0.000,000,1 mm, no such direct investigation with our senses is possible. Start with our imaged 1 mm object and let us pretend that we can expand the atoms for which it is made of. How large would the object be before we could see and feel the atoms? The answer is: the size of a mountain. The object would need to be 10 km wide in order for its atoms to be 1 mm. Needless to say, atoms are small.

It does not stop there. In the center of the atom lives the atomic nucleus. Here we talk about a size of 0.000,000,000,01 mm. Now it becomes really crazy, our 1 mm object would need to expand into the size of a giant planet like Jupiter, about 100,000 km across, in order for the atomic nuclei to be available for our senses.

The nucleus is hiding deep inside the atom and does not participate in our everyday life. So, should we care about the nucleus if it does not affect us? Of course! The stability of an atom is solely determined by the nucleus. Hence, the properties of the nucleus decide which atoms Nature has to play around with when building up our world.

The heaviest nucleus which is completely stable is led with 82 protons. However, uranium with 92 protons has a half-life (the time it takes for half of all atoms in a given amount to decay) of 4.5 billion years. This is on a geological time scale and therefore uranium is the heaviest element to be found on Earth. Heavier elements have been produced in the laboratory. The record holder up to this date is the element oganesson with 118 protons. Its half-life has not yet been exactly measured but is near or below 0.001 seconds.

It is not fully understood how heavy elements are formed in the Universe. Light elements, up to iron with 26 protons, are produced through fusion, the merger

of lighter elements, in large enough stars. However, it costs energy to produce even heavier elements. Hence, where in the Universe are there enough available energy to produce these elements? Two suggestions are: in supernovae and in neutron star merges. It seems like in those violent events there are enough of energy to produce elements far beyond uranium. With time, those elements will decay to the well known elements found here on Earth. However, to really understand where and how these processes occur, a good theoretical model is desired. Only then can we really say where all atoms, and by extension ourselves, come from.

There are no microscopes that would allow us to see the atomic nuclei. So, do we humans have any hope in investigating and geting knowledge about this microscopic world? Indeed we have! With the interplay between scientific experiments and theories, step by step is taken towards the discovery and understanding of the atomic nucleus. This is the mission of Nuclear Physics.

The Content of this Thesis

Unfortunately, it has been notoriouly difficult to create a useful model for a detailed description of nuclei heavier than uranium.

The atomic nucleus is a quantum mechanical system and as such, its full description is encoded in its so called wave function. Quantum mechanics describes how the wave function for a nucleus can be obtained from the basic interaction between its protons and neutrons. But the exact interaction is not known and the guessed ones are usually to complicated to find the wave function for a heavy nucleus. However, as a first step, one can focus on properties that depend on the nucleus as a whole. Thus, it is a common practice to treat the interaction between all pairs of particles in an average way and neglect the details of the individual particles. With this technique one can describe the nucleus when it is calm and not energetic.

The main theme in this thesis is to propose a model to go beyond the average treatment and obtain a wave function that can be used to extract high energy and dynamical properties.

The proposed model starts from the average picture. In extension to that, a small extra interaction between all particles is added. This is in no way the exact true interaction; rather it is an interaction that should mimic the true one as good as possible but at the same time be simple enough in order to be useful for heavy nuclei.

The strength of the added interaction is adjusted such that it reproduces the results obtained from the average picture in a regime where that picture is efficient. But with the added interaction one can go beyond the average description and calculate high energy and dynamical properties. Furthermore, because the proposed interaction is simple enough, the model can be used to actually obtain a wave function for heavy nuclei beyond uranium.

We have come a long way from our 1 mm object that we started with. Indeed, with physics and mathematics we can free our brains from the limitations of our senses.

Part I

Introductory Framework

Context and Methodology

Chapter 1

Introduction

Historical Context and Motivation for The Model Presented in this Thesis

It's best to know what you're looking for before you start looking for it.
— Winnie-the-Pooh

This thesis is dedicated to the construction of a novel model which is aimed to describe the structure of heavy and super-heavy atomic nuclei. The model gives as output the nuclear spectra and the corresponding wave functions expressed in the laboratory system. The wave functions can be further used to calculate observables; such as electromagnetic transitions.

The model is based upon a mean-field description of the nucleus obtained from an energy density functional. With that starting point, an effective Hamiltonian is constructed. This Hamiltonian mimics the energy density functional as good as possible but, at the same time, is simple enough to have acceptable calculation times when applied to super-heavy nuclei. Nuclear spectra and wave functions are obtained in beyond-mean-field calculations by the techniques of projections onto good quantum numbers and the generator coordinate method.

In the future, this model could contribute to the search of answers to questions like: Does the Island of Stability exists and is it possible to reach? How are the heavy elements produced in the Universe? Is there a $\mathcal{CP}$-violation beyond the Standard Model of Particle Physics which contributes to the matter anti-matter asymmetry in the Universe?

1.1 Nuclear History

1.1.1 The Periodic Table of Elements

In 1869 Dmitri I. Mendeleev introduced the *Periodic Table of Elements*. It showed a periodicity in chemical properties when the elements where ordered by atomic weight. Immediately two questions arose: What causes the periodicity? What are the boundaries of the table?

At the time, there where no knowledge about the internal structure of the atom and none of its constituents, electrons, protons and neutrons, had been discovered. Actually, the very existence of atoms, not just as an idea, was not yet accepted. Hence, the time was not mature enough to answer these questions.

In the original table the lightest element was, as it is today, hydrogen and it was the only element in the first row. The heaviest ones where thorium and uranium which where the only known elements in the seventh row as we put up the table today. At the time, it was perfectly valid to hypothesize about elements both lighter than hydrogen and heavier than uranium.

However, with the discovery of the electron (J.J. Thomson, 1897), the atomic nucleus (Rutherford, 1911) and the proton (Rutherford, 1917) it was realized that an elements position in the table was determined by the number of electrons around the nucleus. This is, as it is known today, equal to the number of protons in the nucleus. At that time there was an ambiguity if there where additional protons and electrons in the nucleus to make up for the atomic mass. This mass problem was not solved until the discovery of the neutron (Chadwick, 1932). It became clear that the chemical properties of the atoms where solely determined by the number of protons in the nucleus and not by the atomic mass.

Finally, in 1913, Niels Bohr came up with a quantum model of the atomic structure that could answer the first question: Where does the periodicity come from? He postulated that the electrons where forced to move only in some specific orbitals around the nucleus. It is the electrons near the surface of the atom that participate in chemical reactions. Hence, the elements in the same group, which have similar chemical properties, have the same number of electrons in their outermost orbital.

Since hydrogen only has one proton in its nucleus even lighter elements could be ruled out. However, the existence of heavier elements than uranium with its 92 protons, transuranium elements as these would be called, was not yet clear. In 1922 Niels Bohr in his Nobel lecture [1], for the prize he achieved for his atomic

model, includes the element with 118 protons in the periodic table; even though he does not mention the element explicitly in the text. Furthermore, he uses his model to predict its electronic structure; indicating it would be a noble gas.

It was not until the early 1940:s that the question about the existence of transuranium elements finally was answered definitely. It was done by the man-made productions of the elements neptunium, with 93 protons, and plutonium, with 94 protons. Since then, the quest of producing increasingly heavier elements has continued. The record today is 118 protons which is the very element that Niels Bohr included in his Nobel Lecture: oganesson [2]. This element completes the seventh row in the periodic table.

1.1.2 The Nuclear Chart and its Boundaries

The attraction between protons and neutrons, or nucleons with a common word, is caused by the *Strong Nuclear Force*. This force is short ranged; basically acting only between neighboring nucleons. In contrast, the repulsive electric force between protons are long ranged. Therefore, for a large enough nucleus the repulsion will win; the nucleus undergoes fission. Adding neutrons will increase the stability. However, too many neutrons will result in a β^--decay, which is a neutron that turns into a proton, with subsequent fission. Hence, the question arises, which is the heaviest possible nucleus?

In Fig. 1.1, taken from Ref. [3], shows the *Nuclear Chart*. It contains all known nuclei; both those found in Nature and the man-made ones. The stable nuclei are indicated by black squares.

Up to this date, around 3300 nuclei are known. Of course, it would be highly interesting to know how many nuclei, in principle, that could exist.

For a given number of protons there is an optimal number of neutrons; too many or too few will result in a β-decay. The optimal number for each element defines the β-stability line; here the stable isotopes are located. Hence, the Nuclear Chart is bounded to the left and to the right because of the increasingly faster β-decays of the nuclei farther away from the β-stability line.

In the upper part of the Nuclear Chart, due to the large electrostatic frustration, the main decay modes are α-decay and spontaneous fission. This because those modes are governed by the electromagnetic force which is stronger than the weak force which is responsible for the β-decay.

Uranium is the heaviest element to be found in Nature because it happens to

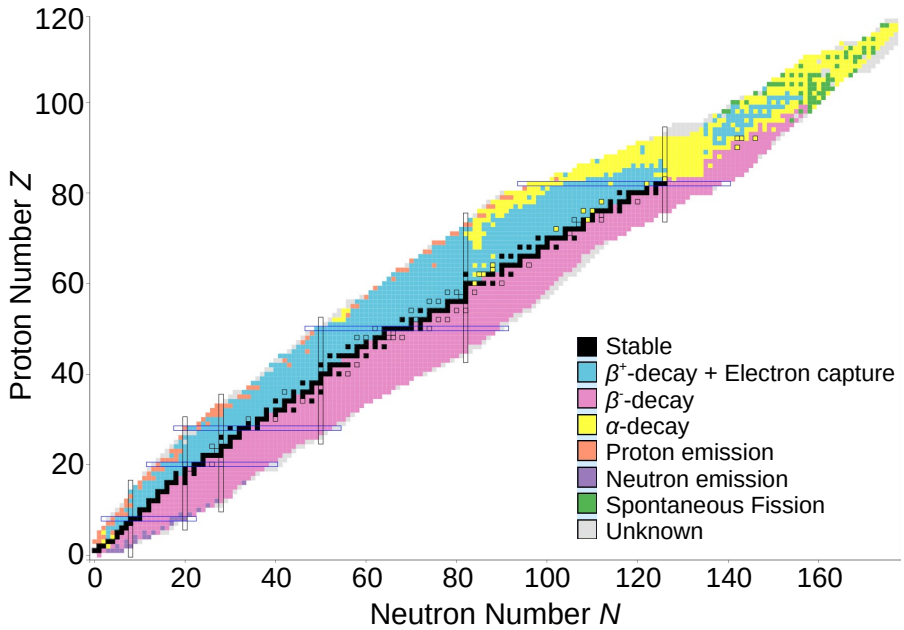

Figure 1.1: The Nuclear Chart. All known nuclei positioned at the numbers of neutrons N and protons Z of which they consist. The colors indicate the main mode of decay which is displayed in the labels. The elements with open black squares have lifetimes comparable to the age of the Universe. The bars show the locations of the magic numbers. The picture is taken from Ref. [3].

be the heaviest element that is stable during cosmological and geological time scales. However, beyond uranium lies the region of *Super-Heavy Nuclei* (SHN); often defined as nuclei with more than 104 protons. Exploration of this region will most likely lead to a deeper understanding of the nuclear structure of exotic elements and the boundaries of the Nuclear Chart.

Experimental research of SHN gives anchor points for theoretical models which otherwise needs to relay on large extrapolations. A theoretical research of SHN can guide experiments to pin down which isotopes to collide, and at which energy, in order to create new elements.

1.1.3 The Island of Stability

It has been a long time strive to discover, both theoretically and experimentally, the so called *Island of Stability*. The name refers to the possibility to have long-lived nuclei, perhaps at a human time scale or even longer, well beyond uranium. This possibility comes from the fact that nuclei have a shell structure. When a

shell is fully occupied the nucleus is especially stable. The proton numbers, Z, and neutron numbers, N, for which this happens are called *magic*. The magic numbers are shown with bars in Fig. 1.1. The highest magic numbers that are found in nature are $Z = 82$ and $N = 126$. These two numbers are combined in the element lead. Hence, lead is double magic and the heaviest stable nucleus. The Island of Stability should concentrate around the next double magic nucleus. But which one is it?

Since the 1960:s it has been known that mean-field models, for example based on Woods-Saxon potentials [4] and modified oscillator potentials [5], predict the magic numbers $Z = 114$ and $N = 184$. More modern mean-field models push the proton magic number as far as to $Z = 126$ [6].

1.2 Experimental Motivations for The Model

The progress made in the experimental study of SHN forces theory to keep up. Improved models are needed in the region of SHN in order to guide experiment towards the production of ever heavier isotopes and to interpret the experimental data.

1.2.1 Recent Experimental Investigations

In recent years, the group of nuclear experimentalists at Lund University has performed a series of experiments aimed to investigate the nuclear structure of SHN.

We, the group of nuclear theory at Lund University, want to contribute to the study of SHN with accurate calculations for the nuclear structure.

The α-decay ^{219}Ra $\rightarrow ^{215}$Rn – A Stepping Stone

As a built up for the experiments on SHN, an experiment for the α-decay of ^{219}Ra to the daughter ^{215}Rn was performed; see Paper I. The study of this process has several motivations. For one thing, the nucleus ^{219}Ra is one of the most short-lived α-decayers. Also, it has been a debate about the ground state spin of ^{219}Ra; either it is $7/2^+$ or $11/2^+$. Both these values are in conflict with the spherical mean-field value of $9/2^+$, where the odd neutron is located in the $g_{9/2}$-shell, and with the strong coupling limit of $5/2^+$, in which the total spin is

equal to the projection onto the symmetry axis. Furthermore, ^{219}Ra lies in or near the region where static octupole deformations are likely to exist. Finally, ^{219}Ra has potentially an isomeric state which can contribute to the α-decay.

The experimental research suggested the ground state spin for ^{219}Ra to be $7/2^+$ and proposed a new decay scheme involving the isomeric state.

The theoretical study of ^{219}Ra investigated the octupole deformation, the proposed α-decay from the isomeric state and the spectrum.

In order to confirm the possibility for a static octupole deformation of ^{219}Ra the code HFBTHO v2.00d [7] was used. This code performs a self-consistent mean-field calculation with an energy density functional. A mean-field treatment does indeed give bulk properties such as the deformation.

For the interpretation of the experimental results, the α-decay rates, from the ground state and the isomeric state of ^{219}Ra into the two lowest lying states in ^{215}Rn, where calculated with the method in Ref. [8]. However, in order to understand the ground state spin of ^{219}Ra, a deeper investigation of the spectrum was needed. For this the many-particle+rotor model [9] was used. In this model a number of valence nucleons are described within a rotating mean-field potential. With this method, the ground state spin of ^{219}Ra can be understood as emerging from configuration mixing.

Flerovium α-decay Chains – Passing through Z =114

By the same experimental group, experiments on SHN have been performed. These are described in Papers II, 3 and 4. Especially, the experiments studied α-decay chains that runs through the anticipated shell gap at $Z = 114$.

By measuring the released energy for each α-particle, Q_α, one can get information about the nuclear structure. A relative high Q_α-value down to $Z = 114$ and a low one down to $Z = 112$ would point towards a shell gap. However, no such behavior was found. But, indeed, the highest neutron number was $N = 176$; eight short from the expected magic number.

In connection to these experiments, we used the newly developed model in order to calculate the spectra for four isotopes of $_{112}$Cn.

1.2.2 Theoretical Considerations

The main theoretical tools for the investigation of heavy nuclei are mean-field models. The bare two-nucleon interaction, known from scattering experiments, can not be directly used; it becomes modified in the nuclear medium. Instead, effective microscopic interactions are used. These interactions have free parameters which are fitted to experimental data of some kind. This data is often of a static nature such as masses and radii. With this approach one can obtain bulk properties of nuclei with high precision [10]. However, for more detailed properties, such as the spectra, transitions and stability of SHN, the mean-field models are not accurate enough to make precise predictions.

Motivated by the frontiers in the experimental research for the structure of SHN, this thesis presents a model which is based upon mean-field models with effective microscopic interactions. It refines those models by converting the mean-field results into a Hamiltonian which can be used within a many-body framework in a straightforward way. In the end, the final results, such as spectra and wave functions, are obtained in the laboratory system.

Chapter 2

Nuclear Theory

Experiment Reveals Nature
Theory Understands Nature

To the uneducated, an A is just three sticks.
— Winnie-the-Pooh

The quest to gain a detailed theoretical understanding of the atomic nucleus has been proven to be hard to achieve. One reason for this is due to the fact that the bare interaction between two nucleons is numerically ill-behaved; mainly because of the impenetrable hard core of the nucleons at small, but finite, distances. Also, the interaction is altered inside the nuclear medium in a not fully controlled manner. A second reason is due to the large amount of particles which build up the nucleus but not large enough to allow for the use of statistical mechanics. In addition, the nucleus is held together by itself. There are no dominant central force for which a residual force can be treated perturbatively as for the electrons in an atom.

2.1 Theoretical Frameworks – An Overview

The best medicine against being fooled?
Knowledge!
— Shellman

2.1.1 From a Microscopic Start and Upwards

This is the bottom to top approach. It starts with some microscopic constituents from which the nuclear properties are derived.

From First Principles – QCD

Maybe the most straightforward and satisfying method to describe nuclei would be to derive all properties from first principles. That is, from the theory of *Quantum Chromo-Dynamics* (QCD). This is the well-established theory for the interaction between quarks and gluons which are the building blocks of nucleons.

However, in the low energy regime of nuclear physics QCD is non-perturbative due to a large coupling constant. Instead, one needs to rely on *Lattice*-QCD (L-QCD). Here one introduces a finite and discretized space. In that way, cut-offs both at the ultraviolet and the infrared ends follows in a natural way. With this technique, it has been possible to determine single-nucleon properties such as coupling strengths to the week axial current [11] and masses [12].

Despite the success for single nucleons, L-QCD has not yet been useful for systems of two or more nucleons [13]. In the near future, L-QCD may be successful for two-nucleon systems. However, it is not realistic for L-QCD to ever be used to describe emergent nuclear phenomena. Even though, it would be fruitful to have a bridge between QCD and effective field theories.

Effective Field Theory

In an *Effective Field Theory* (EFT) one sees nucleons and pions as the basic degrees of freedom; in contrast to quarks and gluons in QCD. This is motivated by the confinement; only colorless objects can exists in the low energy regime. The starting point of EFT is the most general Lagrangian which respects fundamental symmetries stemming from QCD. Furthermore, the terms are ordered

in size based on the energy scale for which the EFT is expected to break down. In this way, one has control over the approximations.

Up to this day, the interaction strengths are fitted to experiment. Hence, the connection to QCD is just qualitative through the symmetries. In the future it may be possible to derive those quantities from L-QCD; making a more direct link between QCD and nuclear physics. One of the most prominent EFT are the *Chiral*-EFT. It is based on the approximate chiral symmetry between up and down quarks; the quark masses are much lower than the nucleonic mass.

Unfortunately, EFT is currently restricted to light nuclei due to the heavy computational cost that comes with a many-body system.

2.1.2 From a Macroscopic Start and Downwards

This is the top to bottom approach. Instead of dealing with the details, one takes a macroscopic point of view and tries to extract bulk properties of the nucleus by considering it as a single object or as some kind of average of the individual nucleons. This perspective reduces the computational cost greatly; especially for heavy nuclei.

The Liquid Drop Model

In the far end of the macroscopic view lies the *Liquid Drop Model*. Already in the early days of nuclear physics, it was experimentally found that the binding energy per nucleon was rather constant: around 8 MeV. This indicates that the nuclear force is short ranged. A nucleon only feels its immediate neighbors and do not know about the rest of the nucleus apart from the Coulomb force. Other facts, known from scattering experiments, are that the nuclear density is independent of the number of nucleons and that the nuclear surface is rather sharp. Those observations, short range force, constant density and a sharp surface, point at the similarity between a nucleus and a liquid drop. In both systems, a particle in the interior does not feel any net force whereas a particle at the surface is pulled towards the center which gives rise to a surface tension. It is interesting to notice that the surface tension of nuclei is in the order of 10^{18} stronger than that of water.

The liquid drop model is mathematically described by the *Semi-Empirical Mass Formula* which gives the binding energy for given numbers of neutrons and protons. The formula was developed by Weizsäcker [14] and Bethe and Bacher [15].

With this simple and intuitive model one can get accurate predictions for the average behavior of ground state properties throughout the Nuclear Chart. For example, binding energies and the beta-stability line are well described. Also fission barriers can be calculated; putting an upper bound on Z for which heavier elements would undergo spontaneous fission.

The liquid drop model is a classical theory with no spectrum; only ground state properties. A spectrum can be obtained by quantizing vibrations and rotations. With this method it is possible to derive the *Bohr Hamiltonian* [16] which can be solved by the *Schrödinger Equation*.

The Shell Model

It was found in the 1930:s that nuclei with a specific number of protons and/or neutrons are especially stable. This means that they have higher binding energy than expected from the semi-empirical mass formula. Those numbers became known as magical and they are: 2, 8, 20, 28, 50, 82 for both protons and neutrons and additional 126 for neutrons; see Fig. 1.1. Thus, these nuclei resemble the behavior of the noble gases in the periodic table of elements. This leads to the conclusion that there is a shell structure for the nucleons inside a nucleus in very much the same way as for the electrons inside an atom. The *Shell Model* was born.

The atom is held together by the potential stemming from the Coulomb interaction which is exactly known. This is not the case for the nucleus. Hence, the first shell models simply guessed the form of the potential. From the short range nature of the nuclear force, leading to a liquid drop behavior of the nucleus, the potential felt by a nucleon is expected to be flat near the nuclear center and steep at the nuclear surface.

The first shell model that reproduced all known magic numbers where made by Maria Goeppert Mayer and J. Hans D. Jensen [17, 18, 19]. In order to achieve this, they used an isotropic potential, either an infinite square well or a harmonic oscillator, with a strong spin-orbit coupling.

A more realistic, and somewhat intermediate, alternative to the infinite square well and the harmonic oscillator is the *Woods-Saxon Potential* [20] which has the form of a Fermi function. However, this potential has no analytical solutions.

The isotropic shell model works well for nuclei close to magic numbers. However, it does not succeed that well for nuclei in between magic numbers. The reason for this is *nuclear deformation*.

The Nilsson Model

In the 1950:s evidence for rotational bands started to show up in experiments. Such a band is a sequence of states with angular momenta $I = 0, 2, 4, 6, ...$ (in units of $\hbar$) with energies proportional to $I(I+1)$. This is the expected behavior of a rotating body with a static deformation. In addition, large electric quadrupole moments and associated strong transitions where found. The large values can not be explained as coming from single particles alone. Instead, the deformation of the nucleus as a whole comes into play.

With this knowledge, Sven Gösta Nilsson improved upon the existing shell model by introducing the deformed and modified oscillator potential [21]. This is an anisotropic potential which is flattened near the center. This is today known as the *Nilsson Model* and with this one can calculate both binding energies and deformations for all nuclei in a satisfactory way.

Shell models typically assume no residual interactions between particles apart from the common potential. This is the view of independent particles for which all interactions are captured in the average potential.

Configuration Interaction

A way to incorporate residual interactions between nucleons is to adopt an effective interaction in a valence space around the Fermi level. The technique is to assume a frozen core of nucleons filling up closed shells. For the rest of the nucleons, the valence nucleons, an effective Hamiltonian is applied; preferably derived from a realistic nucleon-nucleon interaction. This Hamiltonian is then solved within the space of all possible single-particle configurations of the valence nucleons in the chosen valence space. See, for example, Ref. [22] for a review.

In the limit where all nucleons are considered as valence nucleons one arrives at the *No-Core Shell Model*. The first successful calculations for the no-core shell model where made in the 1990:s for light nuclei [23].

2.2 Established Theory used within The Model

I don't believe anything that I don't know.
— Shellman

2.2.1 Self Consistent Mean-Field Models

The potentials which are used in shell models and in the Nilsson model are introduced by hand. They are usually chosen such that they resemble the effects of the short range nature of the nuclear force and at the same time are simple enough to be useful in calculations. Remarkably, these potentials can, with the inclusion of a spin-orbit coupling, reproduce the magic numbers of nuclei.

However, it would be more satisfactory, and perhaps more accurate, to derive the average potential from a microscopic interaction between the nucleons. This can be done within *Self Consistent Mean-Field Models*.

These models are based upon the assumption that all the complex interactions between all the nucleons in a nucleus can be approximated as if the nucleons moved independently in a common potential: the *Mean-Field*. The aim is to derive the mean-field directly from a nucleon-nucleon interaction; instead of putting it in by hand.

Hence, the true interaction is assumed to be well approximated with a single-particle potential. This implies that the total Hamiltonian, H, can be written as a sum of one-body Hamiltonians, h; one for each nucleon.

The Hartree-Fock Method

In the *Hartree-Fock* (HF) method the many-body state for A nucleons, that should approximate the true state as good as possible, is taken to be

$$|\mathrm{HF}\rangle = \prod_{i=1}^{A} a_{k_i}^{\dagger} |0\rangle \tag{2.1}$$

which is known as a *Slater Determinant*. Here $|0\rangle$ is the bare vacuum and $\{a_k^{\dagger}\}$ are single-particle creation operators which place one particle in state k.

From energy minimization in the space of Slater determinants, the HF-method gives the single particle spectrum as a result. The energies and states are the

solutions to the single-particle Schrödinger equation

$$h\,|k\rangle = e_k\,|k\rangle \tag{2.2}$$

with $|k\rangle \equiv a_k^\dagger\,|0\rangle$ and $\{e_k\}$ being the single-particle energies. The corresponding creation operators can be written as the linear combination

$$a_k^\dagger = \sum_l D_{lk} c_l^\dagger \tag{2.3}$$

where D is a matrix of complex numbers and $\{c_l^\dagger\}$ are the creation operators for a predefined single-particle basis. A convenient choice is 3D harmonic oscillator states.

One way to find h from H is to express the HF-energy

$$E^{\mathrm{HF}} = \langle \mathrm{HF}|H|\mathrm{HF}\rangle \tag{2.4}$$

as a functional of the density, $E^{\mathrm{HF}}[\rho]$, where

$$\rho_{ij} = \langle \mathrm{HF}|c_j^\dagger c_i|\mathrm{HF}\rangle = \sum_k D_{ik} D_{jk}^*. \tag{2.5}$$

Minimizing $E^{\mathrm{HF}}[\rho]$ in the space of Slater determinants allows for the identification of the matrix elements $h_{ij} = \langle i|h|j\rangle$ as

$$h_{ij} = \frac{\partial E^{\mathrm{HF}}[\rho]}{\partial \rho_{ji}}. \tag{2.6}$$

See Ref. [24] for details.

The Hartree-Fock-Bogoliubov Method

The nucleons inside the nucleus tend to form pairs coupled to $I = 0$. This is the so called *pairing*. Hence, the nucleons within a shell can not be seen as totally independent since they tend to pair up in time-reversed states. However, this effect can be incorporated in a mean-field model with the *Hartree-Fock-Bogoliubov* (HFB) method [25].

In the HFB-method so called quasiparticles are introduced. These are linear combinations of particles and holes. The corresponding creation operators are written as

$$\beta_k^\dagger = \sum_l U_{lk} a_l^\dagger + V_{lk} a_l \tag{2.7}$$

where U and V are matrices of complex numbers.

An HFB-state, $|\phi\rangle$, is defined to be a vacuum with respect to all quasiparticles. This implies that

$$\beta_k |\phi\rangle = 0 \qquad \forall\, k. \tag{2.8}$$

Explicit, $|\phi\rangle$ can be written as a product of quasiparticle annihilation operators acting on the bare vacuum. That is

$$|\phi\rangle = \prod_k \beta_k |0\rangle \tag{2.9}$$

where the product runs over all k such that the state does not vanishes.

In an HFB-state pairing correlations are built in. There always exists a single-particle basis, the so called canonical basis, in which the HFB-state can be expressed as a linear combination of time-reversed pairs.

Define a general two-body Hamiltonian as

$$H = \sum_{ij} t_{ij} a_i^\dagger a_j + \frac{1}{4} \sum_{ijkl} \bar{v}_{ijkl} a_i^\dagger a_j^\dagger a_l a_k \tag{2.10}$$

where t represents the kinetic energy and $\bar{v}_{ijkl} = \langle ij|v|kl\rangle - \langle ij|v|lk\rangle$ is an antisymmetrized matrix element of a two-body interaction v. Minimizing the energy in the space of HFB-states, with a constraint on the average particle number, ends up in the HFB-*Equations*. In matrix form, these can be written

$$\begin{pmatrix} h & \Delta \\ -\Delta^* & -h^* \end{pmatrix} \begin{pmatrix} U & V^* \\ V & U^* \end{pmatrix} = \begin{pmatrix} U & V^* \\ V & U^* \end{pmatrix} \begin{pmatrix} E & 0 \\ 0 & -E \end{pmatrix} \tag{2.11}$$

where Δ is the pairing field, defined by

$$\Delta_{ij} \equiv \frac{1}{2} \sum_{kl} \bar{v}_{ijkl} \kappa_{kl}, \qquad \kappa_{kl} = \langle \phi | a_l a_k | \phi \rangle \,, \tag{2.12}$$

and E is a diagonal matrix containing all quasiparticle energies. This means that the one-quasiparticle state $\beta_k^\dagger |\phi\rangle$ has the excitation energy E_k relative to the HFB-vacuum $|\phi\rangle$. The single quasiparticle Hamiltonian becomes $h = t + \Gamma - \lambda$ where λ is a Lagrange multiplier for the particle number and Γ is the self-consistent field which is defined as

$$\Gamma_{ij} \equiv \sum_{kl} \bar{v}_{iljk} \rho_{kl}, \qquad \rho_{kl} = \langle \phi | a_l^\dagger a_k | \phi \rangle \,. \tag{2.13}$$

2.2.2 Symmetry Breaking

The mean-field methods usually give rise to a spontaneous symmetry breaking. That is, the solutions do not have the symmetries of the underlying interaction. Indeed, having the freedom of breaking symmetries during energy minimization gives the possibility to find a solution with lower energy as compared to when all symmetries are imposed.

One of the most striking symmetry violations is when the energy minimization results in a deformed nucleus; violating the spherical symmetry of the Hamiltonian. This implies that the angular momentum has no definite value.

One could argue for this to be a drawback of the method because a deformed solution can not be an eigenstate to the Hamiltonian. However, it actually provides physical insight to nuclear phenomena. If the deformation is viewed as the nuclear shape in the intrinsic frame, one can understand the emergence of rotational bands which show up in many nuclear spectra. A rotational band is expected for a deformed and rotating body; even though no real motion is present in a stationary state. It seems that heavy nuclei are macroscopic enough for symmetry breaking to be realized and produce macroscopic phenomena.

Also, for the HFB-method, the conservation of particle number is violated due to the mixing of particles and holes. In the low energy regime of atomic nuclei, the Hamiltonian conserves the number of particles. However, by breaking this conservation one can incorporate pairing correlations in a mean-field description.

Both of the broken symmetries of angular momentum and particle numbers can be restored with the techniques of *Projections* as described in Sec. 2.2.7.

2.2.3 Cranking

A deformed nucleus, at the mean-field level, breaks rotational invariance and has therefore no definite angular momentum. However, the mean-field solution is supposed to be an approximation of the true ground state and, for an even-even nucleus, this state has $I = 0$. Thus, one expects the $I = 0$ component of the mean-field state to be the dominant one.

In order to describe the states in the yrast band, which are the states with the lowest energy for each angular momentum, it would be preferable to end up with other angular momenta as the dominant part. This can be done with the method of *Cranking*.

This method was first introduced by Inglis [26]. The idea is to, for a given angular momentum, make a transformation from the lab system into a rotating frame for which the individual nucleon motion is as simple as possible. This frame coincides with the frame in which the mean-field has a static deformation and principal axes along the coordinate axes.

The transformation is achieved by adding the term $-\omega\hat{I}_x$ to the Hamiltonian. Here ω is the angular frequency of the rotating frame and $\hat{I}_x$ is the operator for the angular momentum around the x-axis which is taken to be stationary relative to the laboratory system. The added term represents the centrifugal and Coriolis forces experienced in the rotating frame. Now one can solve for $H^\omega = H - \omega\hat{I}_x$ at the mean-field level and obtain the intrinsic wave function $|\phi^\omega\rangle$ which depends on ω.

The wave functions obtained in this way have no good quantum number for the total angular momentum as for any deformed solution. However, the projection of the angular momentum onto the rotational axis, $I_x \equiv \langle\hat{I}_x\rangle$, is a constant of motion. This projection is identified as the collective angular momentum. Added to that, there can be single-particle angular momenta parallel to the symmetry axis. However, neglecting single-particle contributions implies that $I_x \approx I$. Hence, ω is adjusted until the desired value of I is obtained.

The energy in the laboratory system is calculated with the original Hamiltonian from $E^\omega = \langle\phi^\omega|H|\phi^\omega\rangle$.

2.2.4 Nuclear Density Functional Theory

The framework of *Density Functional Theory* (DFT) reformulates quantum mechanics in order to handle multi-particle systems. It was originally developed for electronic systems; suited for solid-state physics and chemistry. Instead of a many-particle wave function, with $3N$ degrees of freedom for N particles, the ground state density, with only 3 degrees of freedom, plays the role as the fundamental quantity. It is a remarkable fact that the ground state density contains as much information as the many-body wave function. This fact is stated as the *Hohenberg-Kohn Theorem* [27]: There is a one-to-one correspondence between the ground state density and the external potential. Since the internal interaction between the particles is universal, the density determines the full Hamiltonian which in turn determines, in principle, all observables of the system.

However, in DFT, the interaction is not represented by a Hamiltonian. Instead,

the interaction is contained in the *Energy Density Functional* (EDF); the total energy is a functional of the density.

Bringing DFT into nuclear physics is not trivial. This is partly due to technical issues that comes within the nuclear medium. Such as two particle species, pairing, spin dependence, a sharp surface and many-body forces. Furthermore, there is also a formal issue due to the lack of an external potential; indeed, the nucleus is a self-bound system. Without an external potential the true ground state density is evenly spread out throughout whole space and contains no information about the nuclear structure. Therefore, one needs to extract the translational part of the nuclear state. But this symmetry breaking makes the connection to DFT no longer straightforward; the Hohenberg-Kohn theorem does not directly apply [28].

But inspired by DFT for electronic systems, the *Nuclear*-DFT approach uses an EDF in favor of a Hamiltonian. Since the exact interaction among the nucleons is not known, the EDF has no explicit connection to first principles and does not necessary correspond to an underlying true interaction. Instead, the parameters are fitted to some experimental data.

2.2.5 Microscopic Effective Interactions

One could imagine to use the bare nucleon-nucleon interaction as the two-body interaction in the HF- and HFB-methods. Unfortunately, this is not possible due to the hard core of nucleons. It is an experimental fact that the nucleon-nucleon potential goes to infinity for distances smaller than 0.4 fm. This leads to instabilities of the methods [24].

In addition, the exact nature of the nuclear force is not captured by the nucleon-nucleon interaction alone. The nucleon-nucleon interaction obtained from experiment gets altered inside the nuclear medium.

Therefore, one introduces *Microscopic Effective Interactions*.

Within an effective interaction, many-body interactions show up in addition to the two-body interaction. This is because approximations, which excludes details in the exact interaction, can be influenced by the presence of other nucleons. However, it has turned out that a three-body interaction is both essential and enough in order to get accurate results.

In principle, the form of an effective interaction can be chosen at will. But usually one wants to fulfill fundamental symmetries of Nature. The most prominent

ones are: invariance under translation, rotation, time reversal, parity inversion, Galilean (or Lorentz) transformation and the exchange of two nucleons of the same type. The requirement to fulfill these symmetries puts strong restrictions on the possible forms of the effective interaction.

2.2.6 The Skyrme Interaction

There are several effective interactions that have been used over the years. A popular one, which is applied in this thesis, is the *Skyrme Interaction* [29]. Skyrme proposed a short ranged two-body interaction which respects the fundamental symmetries. It is expanded up to second order in momentum; assuming higher orders to vanish due to the short range nature of the nuclear force. In addition, Skyrme proposed a zero range three-body interaction.

Based on his originally work, most Skyrme interactions use the so called standard form of the interaction [30]. In coordinate space, this form of the two-body interaction can be written

$$\begin{aligned} V(i,j) = & \, t_0 \left(1 + x_0 P^\sigma\right) \delta\left(\mathbf{r}\right) \\ & + \frac{1}{2} t_1 \left(1 + x_1 P^\sigma\right) \left[\mathbf{k}^{\dagger 2} \delta\left(\mathbf{r}\right) + \delta\left(\mathbf{r}\right) \mathbf{k}^2\right] \\ & + t_2 \left(1 + x_2 P^\sigma\right) \mathbf{k}^\dagger \delta\left(\mathbf{r}\right) \mathbf{k} \\ & + i W_0 \left[\boldsymbol{\sigma}(i) + \boldsymbol{\sigma}(j)\right] \cdot \mathbf{k}^\dagger \times \delta\left(\mathbf{r}\right) \mathbf{k} \end{aligned} \tag{2.14}$$

where $\boldsymbol{\sigma}$ is the spin operator, $P^\sigma \equiv 1/2 \left[1 + \boldsymbol{\sigma}(i) \cdot \boldsymbol{\sigma}(j)\right]$ is the spin exchange operator, $\mathbf{r} \equiv \mathbf{r}(i) - \mathbf{r}(j)$ is the relative coordinate, $\mathbf{k} \equiv -\frac{i}{2} \left[\nabla(i) - \nabla(j)\right]$ is the relative momentum operator (in units of $\hbar$), t_0, t_1, t_2, x_0, x_1, x_2, W_0 are free parameters and δ is the delta function.

The three-body contact term reads

$$V(i,j,k) = t_3 \delta\left(\mathbf{r}(i) - \mathbf{r}(j)\right) \delta\left(\mathbf{r}(j) - \mathbf{r}(k)\right) \tag{2.15}$$

with the free parameter t_3. It can be shown [31] that, within the HF-method for even-even nuclei, this three-body interaction is equivalent with the density dependent two-body interaction of the form

$$V(i,j) = \frac{1}{6} t_3 \left(1 + x_3 P^\sigma\right) \delta\left(\mathbf{r}\right) \rho^\alpha \left(\frac{\mathbf{r}(i) + \mathbf{r}(j)}{2}\right) \tag{2.16}$$

for $x_3 = 1$ and $\alpha = 1$. However, it has been observed that treating x_3 and α as free parameters improves the results compared to experiments; even though the direct connection to the underlying interaction then is lost.

With the three-body interaction written as in Eq. (2.16), one has turned the interaction into an EDF which can be used in the HF- and HFB-methods [32].

The free parameters of the Skyrme interaction are fitted to experiments. Different sets of experimental observables lead to different Skyrme parametrizations. Some commonly used ones may be mentioned.

The SLy4 [33] parametrization is based on a fit for infinite neutron matter which can be used for neutron stars. It is generalized to include finite nuclear matter and fitted to binding energies and charge radii of double magic nuclei.

The SIII [34] parametrization puts $x_3 = 1$ and $\alpha = 1$; corresponding to a true interaction. Also this parametrization uses the binding energies and charge radii as the fitting parameters. However, the fit is done directly for a selection of double magic and semi-magic nuclei.

Of the same spirit is the parametrization UNEDF1 [35]. It does the same type of fit for binding energies and charge radii but, with the use of computational power, applied to 75 nuclei; both spherical and well deformed. Furthermore, the selected nuclei are mostly heavy ones; 47 of them range between $Z = 88$ and $Z = 108$. This parametrization is the most modern one of those mentioned here.

Instead of ground state properties, the SkM* [36] parametrization is based on characteristics associated with collective vibrations; especially charge dipole and monopole vibrations. On top of that, it is fitted to fission barriers in the actinide region: $Z = [89, 102]$.

2.2.7 Beyond-Mean-Field Methods

Using EDF:s in the framework of HFB has been proven to give bulk properties of nuclei, such as binding energies and charge radii, with high accuracy and precision [10].

Despite the success of mean-field methods, and the physical insight they provides, they can not be the complete picture. A true eigenstate should respect all symmetries of the Hamiltonian and only such a state can be properly labeled with good quantum numbers. For example, a deformed state has no definite angular momentum. But in order to get reliable theoretical spectra and to calculate electromagnetic transitions it is crucial to have good angular momentum without the need of extra assumptions

for going from the intrinsic system into the laboratory system. Hence, it is preferable to reach *Beyond-Mean-Field*.

Projections onto Good Quantum Numbers

A many-body state obtained within a mean-field method can, in principle, be written as a linear combination of states which all have good quantum numbers. Hence, one can project out the one with the desired number.

The projection operators presented here are restricted to be acted upon a state with good number parity. This means that the state does not mix even and odd particle number which implies that it also does not mix integer and half-integer angular momenta. This is indeed true for an HFB-state [24].

The projection operator for particle number reads [37]

$$\hat{P}^N = \frac{1}{\pi}\int_0^\pi e^{-i\theta(\hat{N}-N)}d\theta \tag{2.17}$$

where $\hat{N} = \sum_l a_l^\dagger a_l$ is the number operator and N is the number to be projected out. Note that this operator is used for both neutrons and protons individually.

The projection operator onto total angular momentum I and its projection M onto the laboratory z-axis can be written [37]

$$\hat{P}^I_{MK} = \frac{2I+1}{8\pi^2}\int_0^{2\pi} d\alpha \int_0^\pi d\beta \sin(\beta) \int_0^{2\pi} d\gamma D^{I*}_{MK}(\alpha,\beta,\gamma)\hat{R}(\alpha,\beta,\gamma) \tag{2.18}$$

where (α,β,γ) are the three Euler angles, the number

$$D^I_{MK}(\alpha,\beta,\gamma) \equiv \langle IM|\hat{R}(\alpha,\beta,\gamma)|IK\rangle \tag{2.19}$$

is an element of the Wigner D-matrix and

$$\hat{R}(\alpha,\beta,\gamma) = e^{-i\alpha\hat{I}_x}e^{-i\beta\hat{I}_y}e^{-i\gamma\hat{I}_z} \tag{2.20}$$

is the rotation operator with $\hat{I}_i$ being the angular momentum operator along the i-axis.

In the projection operator for the angular momentum, an additional quantum number $K \in \{-I, I\}$ is showing up. In the end, the final state is written as the linear combination

$$|IM\rangle = \sum_{K=0}^{I} g_K^I \hat{P}_{MK}^I |\Phi\rangle \tag{2.21}$$

where the coefficients g_K^I are found from energy minimization. In the case of an axially symmetric nucleus, K can be interpreted as the projection of the total angular momentum onto the symmetry axis.

Note that, in general, the summation over K should start at $-I$. However, for a state with good signature, the states $\hat{P}_{MK}^I |\Phi\rangle$ and $\hat{P}_{M-K}^I |\Phi\rangle$ are identical [24]. Therefore, in this case, the negative K-states do not add anything new.

In a numerical computation the projection operators need to be discretized. How this can be done is shown in App. B.

The Generator Coordinate Method

In the mean-field methods the many-body state is expressed as a single Slater determinant of single-particle or quasiparticle nature. In contrast to that, a many-body state obtained from a beyond-mean-field method is a correlated state; a super position of several Slater determinants. A direct application of this statement gives the ansatz

$$|\Psi\rangle = \sum_a h_a |\Phi_a\rangle \tag{2.22}$$

for the many-body state $|\Psi\rangle$. Here $\{|\Phi_a\rangle\}$ are Slater determinants, which define a many-body basis, with weights $\{h_a\}$. The index a represents all parameters needed in order to characterize the Slater determinant.

This is the starting point for the *Generator Coordinate Method* (GCM). This method was first introduced by Hill and Wheeler in 1953 to describe fission [38]. Directly from the Schrödinger equation one arrives at the *Hill-Wheeler Equation*

$$\sum_a h_a H_{a'a} = E \sum_a h_a \mathcal{O}_{a'a} \tag{2.23}$$

where

$$H_{a'a} = \langle \Phi_{a'} | H | \Phi_a \rangle \,, \qquad \mathcal{O}_{a'a} = \langle \Phi_{a'} | \Phi_a \rangle \tag{2.24}$$

are the matrix elements for the Hamiltonian and the overlap in the many-body basis. From the Hill-Wheeler equation one can obtain the coefficients h_a and the energy E for the state $|\Psi\rangle$.

In principle, any set of coordinates a can be used. However, the method is particular well suited to describe correlations of large amplitude collective motions: vibrations and rotations. In that case, parameters for the nuclear deformation are the ones to be used.

Chapter 3

Description of The Model

Beyond-Mean-Field
by Mapping Nuclear-DFT
into an Effective Hamiltonian

The more you think about it,
the more you realize there are no simple answers.
— Winnie-the-Pooh

Nuclear-DFT is the main tool for the theoretical study of the major part of the Nuclear Chart; from medium mass nuclei all the way up to SHN. The results obtained from Nuclear-DFT have been demonstrated to reproduce experimental data on bulk properties, for example masses, quadrupole moments and radii, with high precision [10]. Those are properties that are associated with static degrees of freedom for the nucleus. However, for properties associated with dynamical degrees of freedom, such as rotations, vibrations and transitions, the results from Nuclear-DFT are not that adequate.

Since Nuclear-DFT necessarily leads to an intrinsic state, not a laboratory state, it breaks fundamental symmetries and does not necessarily have good quantum numbers. So, for example, electromagnetic transitions are forced to be treated in a semiclassical way in this framework. A full quantum treatment requires good angular momenta. That implies

symmetry restoration and the introduction of multi-mean-field states; a beyond-mean-field approach.

The objective of the presentation here is to *describe the construction of a novel beyond-mean-field model applicable to medium mass nuclei all the way up to SHN*. The model is able to produce spectra and proper wave functions. This means that the wave functions are expressed in the laboratory system with good quantum numbers and are accurate enough in order to calculate observables; for example electromagnetic transitions. For the model to be applicable to SHN, it needs to be simple enough to have acceptable calculation times. At the same time, the model has to capture enough physics in order to be a good approximation over more or less the whole Nuclear Chart.

Because of the success of Nuclear-DFT this framework is used as a starting point and is further extended in order to achieve nuclear spectra and proper wave functions.

Since wave functions with good quantum numbers are a desired feature, symmetry restoration is mandatory. In order to capture collective excitations, such as rotational bands, degrees of freedom associated with large amplitude collective motions are included through the GCM. In addition, to capture single-particle excitations, quasiparticle excitations on top of the many-body basis-states within GCM are introduced. That is done in a way that resembles the excitations caused by temperature. This procedure is described in Sec. 3.5.

The model can schematically be described as DFT→GCM+Temp.+Proj.

3.1 Issues with an EDF in GCM and Projections

The use of an EDF within GCM and Projections can give rise to formal and technical issues.

It is a common feature that an EDF, such as the Skyrme interaction, has the two-body interaction written as an expansion up to second order in relative momentum. This expansion serves well for ground state properties where the momentum is low. But it becomes non-realistic for high momentum interactions. Indeed, at the mean-field level the high momentum part is never probed and can safely be ignored [39]. However, in the GCM,

when mixing many-body states, this high momentum regime could give rise to non-physical contributions.

The density dependent part of an EDF, which corresponds to a contact interaction, can cause divergences. Indeed, an exact and analytical treatment of a δ-potential gives an infinite binding energy [40]. Again, the full δ-potential is not probed at the mean-field level whereas it can be so in the mixing process of GCM.

Hence, the use of an EDF in the GCM may require a cut-off in momentum in order to avoid divergences.

Furthermore, the use of the transitional density in off-diagonal elements of the Hamiltonian using the generalized Wick's theorem [41] is inconsistent and can cause divergences [42]. Moreover, introducing approximations in the Hamiltonian, especially neglecting the exchange contribution, can give rise to poles both in the GCM and for projections [43].

In addition to all that, it is not well-defined how to treat the density dependence when mixing two many-body states which, in general, have different densities. Also, turning the density into an operator is not straightforward for $\alpha \neq 1$ in Eq. (2.16). However, several recipes have been proposed for dealing with the density dependence at the beyond-mean-field level [42, 44, 45, 46].

In order to use the success of EDF:s within HFB and extend the framework with the GCM and projections, but at the same time avoid the issues mentioned in this section, our method is as follows: Postulate an effective two-body Hamiltonian with no density dependence. Map results from an EDF into the Hamiltonian. This Hamiltonian can then be used in a straightforward way within GCM and projections. Also, take care to include all exchange terms.

3.2 The Effective Hamiltonian

At the heart of the model lies *The Effective Hamiltonian*: H_{eff}. It is postulated to be a two-body operator with separable interactions which should capture the most important physical effects in atomic nuclei and at the same time be efficient enough to be applicable to SHN.

The Effective Hamiltonian can be divided into three parts as

$$H_{eff} = H_0 + H_Q + H_P. \tag{3.1}$$

Here H_0 is a *spherical single-particle potential* obtained from Nuclear-DFT. This part should capture the bulk properties of the nucleus at the mean-field level. The term H_Q is a *modified quadrupole interaction* that represents the quadrupole deformation. The last part, H_P, contains the *pairing* between nucleons of the same species.

In order to achieve feasible calculation times when applied to SHN, H_{eff} has been chosen as simple as possible. That is, no explicit three-body force and separable two-body forces. However, the interactions have been carefully selected such that H_{eff}, despite its simplicity, still generates accurate results. It is based on a physical insight of the most important degrees of freedom for the atomic nucleus; namely: quadrupole deformation and pairing. Also, it is known that a quadrupole-quadrupole interaction results in a deformed Nilsson potential and therefore gives accurate results at the mean-field level.

The Pairing-plus-Quadrupole Model

The Effective Hamiltonian resembles the *Pairing-plus-Quadrupole Model*.

It was first found by Elliot in 1958 [47] that eigenstates to a quadrupole operator can be used to build up rotational bands. That is done by viewing the eigenstate as an intrinsic state and integrating it over all space angles weighted with Wigner matrices to obtain the laboratory state for given angular momentum.

The concept was further developed by Belyaev [48] by considering an interaction between a single-particle quadrupole moment and the total quadrupole moment of the nucleus: a quadrupole-quadrupole interaction. In addition to that, he included a pairing interaction and therefore introduced the pairing-plus-quadrupole model.

For a review of the Pairing-plus-Quadrupole model and motivations for the same, see, for example, Baranger and Kumar [49, 50], Bes and Sorensen [51] and references therein.

The Normal-Ordered Two-Body Approximation

The form of the Effective Hamiltonian, as a one- and two-body operator, is the same as in the *Normal-Ordered Two-Body Approximation* (NO2B) [52]. It is known that a three-body force is crucial to incorporate in order to get an accurate description of atomic nuclei. However, the three-body part leads to a heavy computational load for beyond-mean-field calculations. But in NO2B a reference state, preferably taken as an HF-state, is introduced. Relative to the reference state, a large part of the full three-body interaction can be incorporated in the one- and two-body parts; the residual part is neglected.

Indeed, the explicit expression of the Hamiltonian in NO2B can be derived, in principle, from a microscopic effective interaction. However, in this work H_{eff} is chosed based on physical knowledge of the most important degrees of freedom for the atomic nucleus and the interaction strength is adjusted such that Nuclear-DFT-results obtained from an EDF are reproduced.

3.2.1 The Spherical Single-Particle Potential

The spherical single-particle potential is written as

$$H_0 = E_0 + \sum_i e_i a_i^\dagger a_i \tag{3.2}$$

where E_0 is a constant and e_i is the single-particle energy for state i with $a_i^\dagger$ (a_i) being the corresponding creation (annihilation) operator. The single-particle spectra is found from a Nuclear-DFT-calculation with a spherical constraint. The constant E_0 is chosen such that the HF-energy (2.4) from H_{eff}, for a spherical shape, becomes equal to the binding energy obtained by the Nuclear-DFT-calculation.

The state i is characterized by the usual quantum numbers for a spherical potential. That is,

$$a_i^\dagger |0\rangle = |\tau_i, n_i, j_i, m_i, l_i, s_i\rangle \tag{3.3}$$

where τ is the isospin ($\tau = p$ for protons and $\tau = n$ for neutrons), n is the principal quantum number, j is the total angular momentum with the projection m on the z-axis, l is the orbital angular momentum and s is the spin of the nucleon. Note that $s = 1/2$ for all nucleons and can therefore be omitted. Also, as a consequence of that, $j = l \pm 1/2$.

The solution obtained from Nuclear-DFT can be viewed as the reference state within NO2B. When the Hamiltonian is expressed in the single-particle basis of this reference state the major part of the three-body interaction can be captured within one- and two-body operators [52].

3.2.2 The Modified Quadrupole Interaction

The quadrupole operator that originally appeared in the pairing-plus-quadrupole model is

$$\hat{Q}^{2\mu} = r^2 Y^{2\mu} \tag{3.4}$$

where r is the radial coordinate and $Y^{2\mu}$ is a spherical harmonic. This operator works well at the mean-field level but the r^2-dependence is non-realistic far away from the ground state. In Ref. [53] Kumar and Sørensen derive a modified radial dependence of the quadrupole force in a self consistent way. That is, at equilibrium, the density is required to be proportional to the potential. The starting point is a spherical Woods-Saxon potential with the inclusion of a spin-orbit coupling and a Coulomb interaction. Assuming small deformations, the quadrupole interaction is obtained from a first order Taylor expansion of the spherical potential. In addition, the interaction respects the expected symmetries of the nuclear force.

The model in this work uses the radial dependence derived by Kumar and Sørensen with two minor differences which will be described in this section.

The operator for the modified quadrupole interaction can be divided into three parts. That is, using a tilde to distinguish it from the ordinary quadrupole operator,

$$\widetilde{Q}^{2\mu}_{\tau} = \widetilde{Q}^{2\mu}_{\tau,C} + \widetilde{Q}^{2\mu}_{\tau,WS} + \widetilde{Q}^{2\mu}_{\tau,SO} \tag{3.5}$$

which corresponds to the Coulomb interaction, the Woods-Saxon potential and the spin-orbit coupling. Note that there are two separate quadrupole interactions for the two nucleon species which is indicated by the subscript τ.

The Coulomb Interaction

The first term of Eq. (3.5) represents the Coulomb interaction between protons. This term is identical to the one in Ref. [53] and reads

$$\widetilde{Q}^{2\mu}_{\tau,C} = -r\frac{\partial H_C}{\partial r}Y^{2\mu}\,\delta_{\tau p} \tag{3.6}$$

where H_C is the electric potential energy for a single proton. It is taken to be, in SI-units,

$$H_C = \frac{Ze^2}{4\pi\varepsilon_0}\left[\frac{1}{r}\theta(r-R_p) + \frac{1}{R_p}\left(\frac{3}{2} - \frac{1}{2}\left(\frac{r}{R_p}\right)^2\right)\theta(R_p - r)\right] \tag{3.7}$$

where e is the elementary charge and θ is the Heaviside step function. This form corresponds to the electric interaction between one proton and a homogeneously charged sphere of radius R_p and total charge of Ze. The radius R_p is interpreted as the radius parameter for protons: the radius where the proton density is half the maximum value at the center. The radial parameters for both nucleon species are related to the root-mean-square radii and are, in this work, given by

$$R_\tau = 0.9\sqrt{\frac{5}{3}\left\langle r^2\right\rangle_\tau} \tag{3.8}$$

which is the approximate relation for a Fermi distributed density [54]. The expectation value $\langle r^2\rangle$ is calculated from Nuclear-DFT.

The Woods-Saxon Potential

The second term of the modified quadrupole interaction (3.5) is

$$\widetilde{Q}^{2\mu}_{\tau,WS} = -R_\tau W_\tau \frac{\partial f_\tau}{\partial r}Y^{2\mu}. \tag{3.9}$$

It originates from the Woods-Saxon potential with the radial form factor

$$f_\tau = \frac{1}{1+\exp\left(\dfrac{r-R_\tau}{a}\right)} \tag{3.10}$$

where a is the diffuseness parameter, taken to be $a = 0.9$ fm, and R_τ is the radius parameter (3.8). The constant W_τ is the depth of the Woods-Saxon potential and it is given by

$$W_\tau = V_0 \left(1 \pm \kappa \frac{N-Z}{N+Z}\right) \tag{3.11}$$

where the upper and lower signs are for protons and neutrons, respectively. For the values of V_0 and κ the so called universal parameters are used which are applicable throughout the whole Nuclear Chart [55]. The values are $V_0 = -49.6$ MeV and $\kappa = 0.86$. Note that the diffuseness parameter is taken to be larger than in Ref. [55] since the reproduction of the Nuclear-DFT-results became more accurate with the larger value.

In expression (3.9) for ${\widetilde{Q}^{2\mu}_{\tau}}_{WS}$ the radial parameter R_τ appears instead of the radial variable r as it does in Ref. [53]. The reason for this can be traced back to a different kind of stretching of the nucleus. Kumar and Sørensen stretch the nucleus in a continuous way whereas in this work the diffuseness thickness of the nuclear surface is taken to be constant and independent of deformation. This has been investigated in Ref. [56].

The Spin-Orbit Coupling

The third, and last, term of Eq. (3.5) corresponds to the spin-orbit coupling. It can be written as

$$\widetilde{Q}^{2\mu}_{\tau,SO} = \frac{W_\tau v_{so} \lambda^2}{2} \left(\frac{\partial^2 f_\tau}{\partial r^2} - \frac{1}{r}\frac{\partial f_\tau}{\partial r}\right) \frac{1}{2} \left(\boldsymbol{l}\cdot\boldsymbol{s}\, Y^{2\mu} + Y^{2\mu}\, \boldsymbol{l}\cdot\boldsymbol{s}\right). \tag{3.12}$$

The strength of the spin orbit coupling v_{so} and the constant λ are kept from Ref. [53]. Those are $v_{so} = 32$ and $\lambda = \frac{\hbar}{Mc}(1 + A^{-1})$ with the nucleon mass $M = 939$ MeV/c^2.

In this work, as opposed to Ref. [53], the operator is written in a symmetric way. By this, the ambiguity in the ordering of $\boldsymbol{l}\cdot\boldsymbol{s}$ and $Y^{2\mu}$ is avoided; indeed, they do not commute. Furthermore, the operator $\boldsymbol{l}\cdot\boldsymbol{s}Y^{2\mu}$ does not have the same properties under Hermitian conjugation as the spherical harmonics: $Y^{2\mu\dagger} = (-1)^\mu Y^{2-\mu}$. However, the symmetric version has this symmetry. Letting all terms in the modified quadrupole interaction respect that symmetry simplifies the calculations.

The Modified Quadrupole Operator inside The Effective Hamiltonian

The modified quadrupole operator, apart from the Coulomb interaction, acts only at the nuclear surface which can be seen from the derivatives of the form factor. This is a more realistic type of quadrupole interaction than the originally one with its r^2-dependence.

The modified quadrupole interaction in the Effective Hamiltonian reads, when antisymmetrized,

$$H_Q = -\frac{1}{4}\chi \sum_{ijkl} \sum_{\mu=-2}^{2} \left(\widetilde{Q}^{2\mu}_{ik} \widetilde{Q}^{2\mu *}_{lj} - \widetilde{Q}^{2\mu}_{il} \widetilde{Q}^{2\mu *}_{kj} \right) a^{\dagger}_i a^{\dagger}_j a_l a_k \tag{3.13}$$

where $\{\widetilde{Q}^{2\mu}_{ik}\}$ are the matrix elements of the modified quadrupole operator in the basis of single-particle states. These can be written

$$\widetilde{Q}^{2\mu}_{ik} = \langle i|\widetilde{Q}^{2\mu}_{p}|k\rangle \, \delta_{\tau_i,p}\delta_{\tau_k,p} + \langle i|\widetilde{Q}^{2\mu}_{n}|k\rangle \, \delta_{\tau_i,n}\delta_{\tau_k,n}. \tag{3.14}$$

The strength of the modified quadrupole interaction is modulated by χ. This parameter is the only free parameter in H_{eff} and is determined by a fit to Nuclear-DFT-results which is described in Sec. 3.3.

For convenience, a separable form of H_Q is chosen. However, it is important to notice that any nuclear interaction can be written as a sum of separable terms. This sum can formally be found from, for example, a singular value decomposition [57]. Furthermore, the separable terms can be expressed in a multipole expansion; in order to explore the physical degrees of freedom associated with the nuclear shape. Viewed in this way, H_Q can potentially be derived, and extended, from a microscopic effective interaction.

3.2.3 The Pairing Interaction

For the pairing interaction the *Seniority Model* is used. In this model one assumes a constant pairing strength between all time-reversed single-particle states within a window around the Fermi level. These pairs are

$$|j, m\rangle \quad \text{and} \quad (-1)^{j-m}\,|j, -m\rangle \tag{3.15}$$

where all the other quantum numbers are equal. The interaction strength is allowed to be different for protons and neutrons. Therefore, the pairing

Hamiltonian can be written

$$H_P = -\frac{1}{4} \sum_{q\in\{n,p\}} G^q P^q_{ij} P^q_{kl} a^\dagger_i a^\dagger_j a_l a_k. \tag{3.16}$$

Here G^q is the pairing strength between particles of type q and P^q picks out time-reversed states; explicitly it is written as

$$P^q_{kl} = (-1)^{j_l - m_l} \delta_{(\tau nlj)_k,(\tau nlj)_l} \delta_{m_k,-m_l} \delta_{\tau_l,q}. \tag{3.17}$$

The value of G^q is calculated within the *Uniform Model* [54] in which all single-particle levels in the pairing window are considered to be equidistant in energy. From this one can find a relation between the interaction strength and the pairing gap, Δ, which reads

$$\Delta = 2S \exp\left(-\frac{1}{G^q \rho^q}\right) \tag{3.18}$$

where $[-S, S]$ is the pairing window in which the pairing interaction is considered to be active, in this work is $S = 30$ MeV, and ρ^q is the level density for given nucleon species. Empirically it is known that the average pairing gap follows the relation $12\ \text{MeV}/\sqrt{A}$. However, it has been shown [58] that within a particle number projection the experimental values are better reproduced with the scaled version $\widetilde{\Delta} = 0.7 \times \Delta$. The level density is calculated by averaging all single-particle levels within the pairing window. This becomes, in general, different for protons and neutrons.

The pairing strength found from the uniform model reproduces the average pairing gap when it is used within a uniform single-particle spectra. However, when it is used together with a more realistic, non-uniform, spectra the variations in the pairing gaps due to shell structure can be captured.

3.3 Mapping an EDF into The Effective Hamiltonian

A crucial step in the model is to go from an EDF to a two-body Hamiltonian with no density dependence. This is done by adjusting the free parameter χ in the modified quadrupole interaction (3.13) such that it reproduces results obtained from Nuclear-DFT. Since χ represents a quadrupole interaction, the quantity used for comparison is the binding energy as function of the axial symmetric quadrupole moment $\langle \hat{Q}^{20} \rangle$.

Hence, axial symmetric HF-calculations for several constraints on the quadrupole moment is performed; both with an EDF and with H_{eff}. The aim is to let the two curves coincide as good as possible by adjusting χ.

Therefore, the HF-energy (2.4) from H_{eff} with constraints on the quadrupole moment needs to be calculated. Since axial symmetry is imposed, only the term with $\mu = 0$ in H_Q (3.13) contributes to the energy. Additionally, at the HF-level, the pairing interaction is neglected. With this, the HF-energy is given by

$$E^{\mathrm{HF}} = \langle \mathrm{HF}|H_0 + H_Q(\mu = 0) - \lambda \widetilde{Q}^{20}|\mathrm{HF}\rangle \tag{3.19}$$

where λ is a Lagrange multiplier. Note that the constraint is on the modified quadrupole moment instead of the original one; this will simplify the calculations. With the definition of the density $\rho_{ij} \equiv \langle \mathrm{HF}|a_j^\dagger a_i|\mathrm{HF}\rangle$, the HF-energy (3.19) can be expressed as an EDF according to, see Ref. [24],

$$\begin{aligned} E^{\mathrm{HF}}[\rho] = E_0 &+ \sum_i e_i \rho_{ii} \\ &- \frac{1}{2}\chi \left(\mathrm{Tr}\left[\rho \widetilde{Q}^{20}\right] \mathrm{Tr}\left[\rho \widetilde{Q}^{20\dagger}\right] - \mathrm{Tr}\left[\rho \widetilde{Q}^{20} \rho \widetilde{Q}^{20\dagger}\right] \right) \\ &- \lambda \mathrm{Tr}\left[\rho \widetilde{Q}^{20}\right]. \end{aligned} \tag{3.20}$$

The single-particle Hamiltonian (2.6) is calculated as

$$h_{ij} = \frac{dE^{\mathrm{HF}}[\rho]}{d\rho_{ji}} = e_i \delta_{ij} - \chi \left(\mathrm{Tr}\left[\rho \widetilde{Q}^{20}\right] \widetilde{Q}^{20}_{ij} - \left[\widetilde{Q}^{20} \rho \widetilde{Q}^{20}\right]_{ij} \right) - \lambda \widetilde{Q}^{20}_{ij} \tag{3.21}$$

where the fact that $\widetilde{Q}^{20}$ is Hermitian has been used. Having constraints on the modified quadrupole moment makes it possible to combine the second and fourth term. Hence, one can define a new variable that controls the constraint. Make it

$$q \equiv \chi \mathrm{Tr}\left[\rho \widetilde{Q}^{20}\right] + \lambda. \tag{3.22}$$

In this way, the unknowns χ and ρ has been absorbed into a new Lagrange multiplier q. Now h can be solved straightforward if one treats the third term as a first order perturbation which is justified by the fact that this term represents the exchange interaction. Hence, diagonalize

$$e_i \delta_{ij} - q \widetilde{Q}^{20}_{ij} \tag{3.23}$$

to get the zeroth order single-particle spectrum for several values of q. For each single-particle spectrum, and the associated HF-state, both the density and the quadrupole moment can be extracted. Hence, with this procedure, the HF-energy from H_{eff}, Eq. (3.20) with $\lambda = 0$, can be calculated and expressed as a function of the quadrupole moment.

In the end, χ is chosen such that E^{HF}, obtained from H_{eff}, is reproducing the binding energy obtained from an EDF as good as possible. However, since H_Q is derived from a first order Taylor expansion, the results from H_{eff} is expected to deviate from the EDF for large enough deformations. Therefore, only a selected range of the quadrupole moments are considered when fitting χ.

An example for the fit of χ for the nucleus ^{48}Cr is shown in Fig. 3.1. Instead of the quadrupole moment $\langle \hat{Q}^{20} \rangle$ the dimensionless deformation parameter $\beta \equiv \frac{4\pi}{5} \langle \hat{Q}^{20} \rangle / \langle r^2 \rangle$ is used as the variable to plot the HF-energy against. The expectation value $\langle r^2 \rangle$ is obtained from the single-particle spectrum. The Nuclear-DFT-results are well reproduced in the interval $-0.25 \leq \beta \leq 0.50$.

3.4 The Many-Body Basis

With χ fixed, the Effective Hamiltonian is used in the framework of GCM. The many-body wave functions, which are used as basis states in the GCM, are obtained within the HFB-method. The collective coordinates which generate the basis are the deformation parameters β and γ; triaxiality is allowed. A grid of HFB-vacua over the (β, γ)-plane is obtained by having a set of constraints on

$$\beta_x = \frac{4\pi}{5} \frac{\langle \hat{Q}^{20} \rangle}{\langle r^2 \rangle}, \qquad \beta_y = \frac{4\pi}{5} \sqrt{2} \frac{\langle \hat{Q}^{22} \rangle + \langle \hat{Q}^{2-2} \rangle}{\langle r^2 \rangle}. \tag{3.24}$$

From these, the deformation parameters are obtained according to

$$\beta = \sqrt{\beta_x^2 + \beta_y^2}, \qquad \gamma = \arctan\left(\beta_y / \beta_x\right). \tag{3.25}$$

The (β, γ)-plane is sampled as homogeneous as possible. Therefore, inspired by the seeds in a sunflower, the values of the deformation parameters for the n:th basis state goes as $\beta \propto \sqrt{n-1}$ and $\gamma = \sqrt{n-1}\, \varphi$ where $\varphi \approx 137.51^\circ$ is the golden angle.

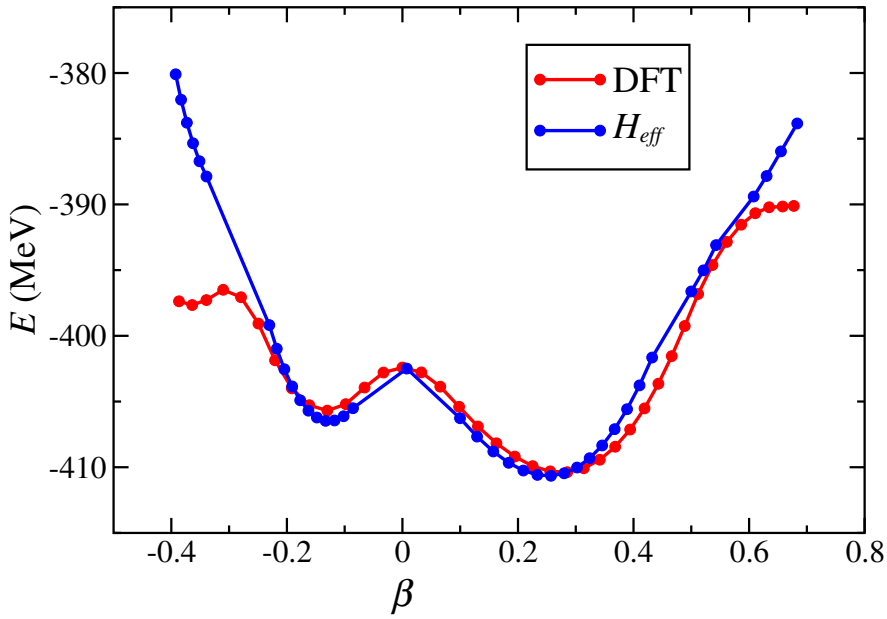

Figure 3.1: Binding energy as a function of the deformation parameter β for the nucleus ^{48}Cr. The energy is obtained at the HF-level; thus no pairing is included. The red curve is from Nuclear-DFT whereas the blue curve comes from the Effective Hamiltonian. This is for the best possible value for χ.

In addition to the deformation, for each grid point, different values for the cranking and for the pairing are used. This is an attempt to include dynamical fluctuations associated with these two degrees of freedom.

In the method of cranking one adds the term $-\omega \hat{I}_x$; see Sec. 2.2.3. In this work, the angular momentum is constrained to $I_x \in \{0, 4, 8\}$ and each point in the grid is assigned one of these values randomly. The corresponding angular frequency ω is estimated by

$$\omega = \frac{\sqrt{I_x(I_x+1)}}{\mathcal{J}_x} \tag{3.26}$$

where $\mathcal{J}_x$ is the moment of inertia around the x-axis for the nucleus. It is estimated in the same way as in Ref. [59].

Dynamics in the pairing within the many-body basis is included by scaling the pairing gaps for both protons and neutrons. This is done by the use of $\widetilde{\Delta}_\tau = g_\tau \widetilde{\Delta}$ in the calculation of G_τ (3.18). In this work the weight is $g_\tau \in \{0.6, 1.0, 1.4, 1.8\}$. For each state in the grid g_n and g_p are individually assigned one of these values randomly.

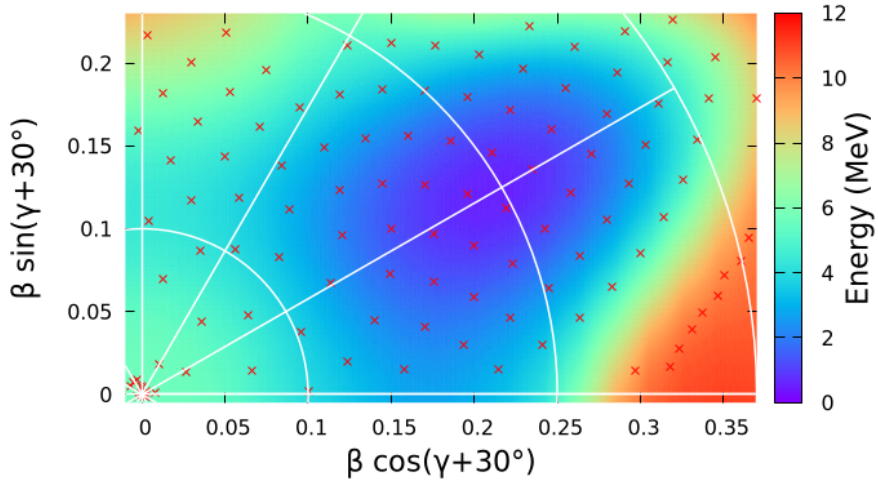

Figure 3.2: The HFB-energy for ^{48}Cr in the (β, γ)-plane. The plane is drawn with the Lund convention: $\gamma = -30°$ along the horizontal axis and $\gamma = 60°$ along the vertical axis. Each cross represents an accepted HFB-state with an excitation energy shown by the color.

For given constraints on β and γ, and fixed values for I_x, g_n and g_p, an HFB-state and its energy is obtained by solving the HFB-equations (2.11) for H_{eff}. Only HFB-states below a certain cut-off in excitation energy are allowed as basis states. In Fig. 3.2 an example for the nucleus ^{48}Cr is shown. Each cross represents an accepted HFB-state with an excitation energy shown by the color. In this calculation, ^{48}Cr has a prolate minimum centered around $\gamma = 0°$ and $\beta = 0.25$.

3.5 Temperature

The chosen collective coordinates account for the dominant collective degrees of freedom in atomic nuclei. Namely: quadrupole deformations, vibrations, rotations and pairing.

However, in addition to the collective degrees of freedom, it would be preferable if the model also could include single particle behavior. This can for example be achieved by, in the many-body basis, including states with quasiparticle excitations built upon the HFB-vacuum. Another way, which is incorporated in this model, is to excite each HFB-vacuum in the many-body basis in a way that resembles the characteristics of *temperature*.

That is, an HFB-vacuum, $|\phi_0\rangle$, is excited into the state

$$|\phi\rangle = \mathcal{N} \exp\left(\sum_{i<j} z_{ij}\beta_i^\dagger \beta_j^\dagger\right)|\phi_0\rangle \tag{3.27}$$

where $\mathcal{N}$ is a normalization constant and $\{z_{ij}\}$ are, in general, complex numbers to be selected. From Thuless theorem [24], this indeed is an HFB-vacuum to some set of quasiparticle operators as long as the matrix z is skew symmetric. In this model a Boltzmann distribution of quasiparticles are required. This is achieved by the choice

$$z_{ij} = \pm e^{-(E_i+E_j)/k_BT} \tag{3.28}$$

where $\{E_i\}$ are quasiparticle energies. The sign is randomly picked for each state and for each matrix element. The temperature k_BT is chosen such that the part of $|\phi\rangle$ which contains the quasiparticle pair with the lowest energy has the weight b compared to $|\phi_0\rangle$. This means that

$$k_BT = -(E_1 + E_2)/\ln(b). \tag{3.29}$$

Note that $|\phi\rangle$ is a mixture of multi-quasiparticle states. Increasing in both the number of quasiparticle pairs and the energy of those pairs but with diminishing weights.

The parameter b can be seen as a convergence parameter which is shown in Fig. 3.3. The figure displays the energy for a selected set of states in the nucleus ^{24}Mg. The solid lines are states in the yrast band. Those states are not improved by the introduction of temperature; indeed, those states are expected to be of a collective nature. In contrast to that, the states above the yrast band, represented by the dashed lines, are improved by the temperature. This is in agreement of the interpretation of those states as quasiparticle excitation on top of the yrast states.

The excited states have an improved convergence in the range $b = [0.3,\ 0.6]$. Therefore, in this work, the value $b = 0.45$ has been picked.

The many-body basis of HFB-states is in general overcomplete. However, by mixing in multi-quasiparticle components into the basis states, together with the random sign in Eq. (3.28), the probability for orthogonal components of the basis states increases. This implies an enlargement of the space spanned by the basis.

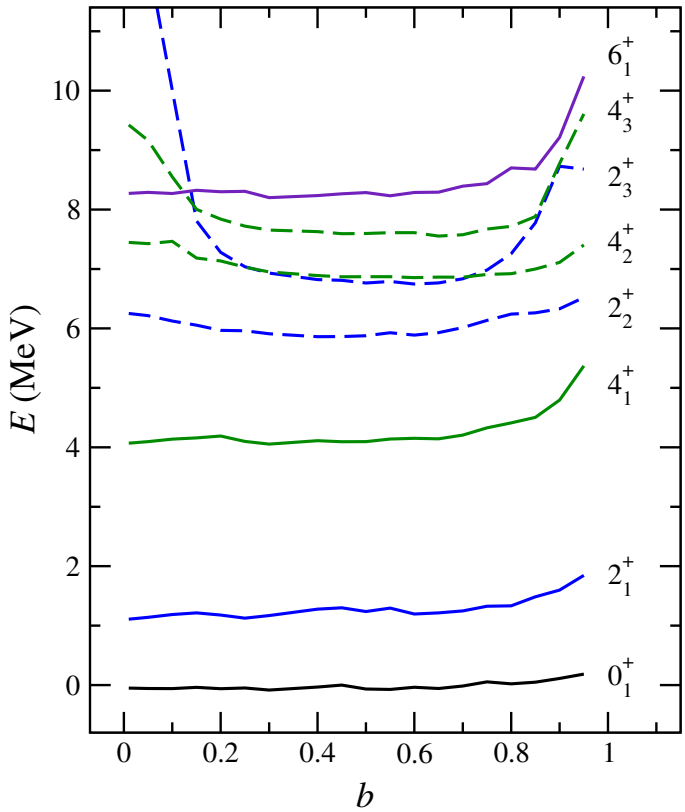

Figure 3.3: The energy for some low lying states in the nucleus ^{24}Mg as a function of the temperature parameter b. The angular momenta and parity for each state are written out to the right of each curve. The solid lines represent states in the yrast band whereas the dashed lines are excited states above the yrast band.

Also, the temperature increases the probability for the basis states to have pairwise non-vanishing overlaps; large enough to be handled by the numeric. This is important in order to have stable calculations in the framework of GCM.

Thus, this temperature inspired mixture of multi-quasiparticle excitations within each many-body basis state has two advantages. First, it will add the features of single particle behavior on top of the collective degrees of freedom introduced by the generated coordinates. Second, it increases the probability for the basis states to be independent and at the same time have pairwise overlaps.

3.6 GCM and Projections

The HFB-method breaks, in general, both the rotational symmetry and the conservation of particles. This results in non-definite angular momentum and particle numbers. These two symmetries can be restored with the technique of projections as described in Sec. 2.2.7.

The projections are performed within the framework of GCM. In GCM, when solving the Hill-Wheeler equation (2.23), the matrix elements of the Effective Hamiltonian and the overlap in the many-body basis are needed. With the inclusion of projections, these elements are [60]

$$\begin{aligned} H_{a'K',aK} &= \langle\phi_{a'}|H_{eff}\hat{P}^I_{K'K}\hat{P}^N\hat{P}^Z|\phi_a\rangle\,, \\ \mathcal{O}_{a'K',aK} &= \langle\phi_{a'}|\hat{P}^I_{K'K}\hat{P}^N\hat{P}^Z|\phi_a\rangle\,. \end{aligned} \tag{3.30}$$

See App. C.1 for the explicit expression for the matrix elements of H_{eff} in the many-body basis. The overlap between two HFB-states has been notorious difficult to carry out. The modulus of the overlap is given by the Onishi formula [24] but the sign remains undetermined. In the context of GCM the relative signs in the overlap matrix is crucial. In order to get the sign correct, we use the expression in Ref. [61]. That expression gives the sign and is, at the same time, numerically stable.

With the matrix elements (3.30), the Hill-Wheeler equation to be solved can be written

$$\sum_{aK} H_{a'K',aK}h^n_{aK} = E_n \sum_{aK} \mathcal{O}_{a'K',aK}h^n_{aK} \tag{3.31}$$

where E_n is the energy for the n:th state and $\{h^n_{aK}\}$ are the corresponding expansion coefficients in the basis of projected HFB-states. Hence, the final state can be written

$$|NZ, IM, n\rangle = \sum_{aK} h^n_{aK}\,|NZ, IMK, a\rangle \equiv \sum_{aK} h^n_{aK}\hat{P}^I_{MK}\hat{P}^N\hat{P}^Z\,|\phi_a\rangle \tag{3.32}$$

where M is the projection of the angular momentum onto the laboratory z-axis and the projected HFB-states have been defined.

3.7 Solving the Hill-Wheeler Equation

In matrix form, the Hill-Wheeler equation (3.31) can be written

$$Hh^n = E_n \mathcal{O} h^n. \tag{3.33}$$

A straightforward way to solve this equation would be to diagonalize $\mathcal{O}^{-1}H$. However, in order to invert the overlap matrix all of its eigenvalues have to be non-zero. Or, equivalent, all basis states have to be linearly independent. This is more often than not the case; the space spanned by the basis is oversampled.

Instead, it is common to create an orthonormal basis by diagonalize the overlap matrix and find the solution to

$$\mathcal{O}u^m = \lambda_m u^m \tag{3.34}$$

where u^m is the m:th eigenvector of $\mathcal{O}$ and λ_m its eigenvalue. From this, one can construct an orthonormal basis of so called natural states

$$|NZ, IM, m\rangle = \sum_{aK} \frac{u^m_{aK}}{\sqrt{\lambda_m}} |NZ, IMK, a\rangle \tag{3.35}$$

for all m for which $\lambda_m \neq 0$. From this procedure, an orthonormal basis in which all projected basis states are contained has been obtained. See Ref. [24] for details.

Of course, in a numerical computation, states for which λ_m is smaller than a certain value needs to be excluded. However, it is not obvious from the start how to choose this cut-off. Instead, in this work, the technique of repeated diagonlization is used. At first, the Effective Hamiltonian is diagonalized within the space spanned by the three natural states with largest λ_m. Then, with decreasing λ_m, one natural state at a time is added and each time H_{eff} is diagonalized. This process continuous until the results become unstable. An indication of convergence is obtained when plateaus for the eigenvalues are formed; when adding more natural states no longer changes the energy.

An example of the procedure is seen in Fig. 3.4. The figure shows the total energy of the yrast states for ^{62}Zn up to $I = 10$ for different sizes of the natural basis. All states above $I = 0$ shows a clear plateau and a sharp break down. The solutions are taken just before the breakdowns; indicated by the crosses.

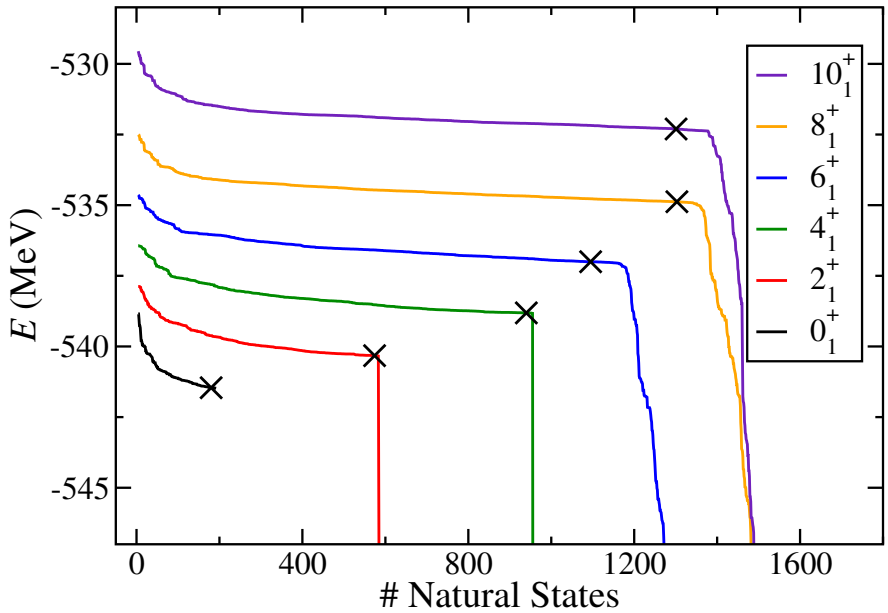

Figure 3.4: Total energy as a function of the number of natural states. The curves correspond to the yrast states in ^{62}Zn. The states are referred to by their angular momentum and parity. The crosses show the location where the final solution has been taken.

In the basis of natural states, H_{eff} can be diagonalized by solving

$$\sum_m \langle NZ, IM, m'|H_{eff}|NZ, IM, m\rangle\, g^n_m = E_n g^n_{m'} \tag{3.36}$$

where g^n is the n:th wave function, expressed in the natural basis, with energy E_n. The matrix element of H_{eff} in the natural basis is given by

$$\langle NZ, IM, m'|H_{eff}|NZ, IM, m\rangle = \frac{1}{\sqrt{\lambda^{m'}\lambda^m}} \sum_{a'K'} \sum_{aK} u^{m'*}_{a'K'} H_{a'K',aK} u^m_{aK}. \tag{3.37}$$

In order to have the final wave function of a given state expressed in the basis of the projected HFB-states (3.32), the Hill-Wheeler coefficients can be extracted according to

$$h^n_{aK} = \sum_m \frac{u^m_{aK}}{\sqrt{\lambda^m}} g^n_m. \tag{3.38}$$

Chapter 4

Electromagnetic Transitions

Putting the Wave Functions to Work

Think, think, think.
— Winnie-the-Pooh

The model presented in this thesis has the ambition to not only produce proper spectra but also to get reliable wave functions. From these one could, in principle, calculate any observable. It has been stated [24] that a proper test for the accuracy of the wave functions are electromagnetic properties such as multipole moments and transition rates. In addition, by studying the interplay between the nucleus and the electromagnetic field one can gain knowledge about the nuclear structure; for example if the angular momentum is of a collective nature or if it has a single-particle behavior.

Therefore, in this chapter, the calculations for transition rates between nuclear eigenstates through the emission of photons will be described. In specific, the focus will lie on transitions in the electric quadrupole channel which are called $E2$-transitions. This channel is common and therefore there exist a large amount of experimental data for which the calculations can be compared to.

Also, with the same procedure, the electric quadrupole moment in the laboratory system is obtained.

4.1 Electric Multipole Moments

The interaction between a nucleus and an external electromagnetic field can be described within a multipole expansion of the nuclear charge. The electric multipoles can be defined as

$$Q^{\lambda\mu} \equiv \int \rho r^{\lambda} Y^{\lambda\mu} d^3r \tag{4.1}$$

where ρ is the charge density and $Y^{\lambda\mu}$ is a spherical harmonic. Written like this, the multipole $Q^{\lambda\mu}$ is the μ:th component of a spherical tensor of rank λ; the components transform into each other under rotations in the same way as the components of the spherical harmonics do. Hence, the value of $Q^{\lambda\mu}$ depends both on the orientation of the coordinate system and on the position of the origin. However, the convention is to place the origin at the center of mass and align the coordinate axes with the principal axes of the nucleus.

The monopole moment ($\lambda = 0$) corresponds to the total charge of the nucleus. The dipole moment ($\lambda = 1$) vanishes identically due to parity conservation; the charge density is forced to be an even function in all coordinates. Hence, the quadrupole moment ($\lambda = 2$) is the lowest non-trivial moment and is the one to be considered in this work.

The expression (4.1) is a classical definition. In the quantum regime the charge density becomes replaced with the probability density and the multipoles are promoted to operators. The electric quadrupole operator can be expressed as

$$\hat{Q}^{2\mu} = \sum_{ij} Q_{ij}^{2\mu} a_i^{\dagger} a_j \tag{4.2}$$

where $\{a_i^{\dagger}\}$ ($\{a_j\}$) are single-particle creation (annihilation) operators and

$$Q_{ij}^{2\mu} = \langle i|\hat{Q}^{2\mu}|j\rangle = e\delta_{\tau_i p}\delta_{\tau_j p} \int \varphi_i^* r^2 Y^{2\mu} \varphi_j d^3r \tag{4.3}$$

is a matrix element of $\hat{Q}^{2\mu}$ in the single-particle basis with wave functions $\varphi_j = \langle \boldsymbol{r}|j\rangle$. Here e is the elementary charge and the Kronecker deltas ensure that only protons contribute to the electric quadrupole moment.

Let $|IM\rangle$ be a nuclear state with good quantum numbers I and M for the total angular momentum and its projection onto the laboratory z-axis,

respectively. Since $\hat{Q}^{2\mu}$ is a spherical tensor operator, the Wigner-Eckart theorem can be used to write its expectation value as

$$\langle IM|\hat{Q}^{2\mu}|IM\rangle = \langle I, M; 2, \mu|I, M\rangle \ \langle I||\hat{Q}^2||I\rangle \tag{4.4}$$

where the first factor on the right hand side is a Clebsch-Gordan coefficient and the second one is the so called reduced matrix element which is independent on both M and μ. From the Clebsch-Gordan coefficient and the angular momentum selection rules, it is seen that the expectation value is identically zero for $\mu \neq 0$ and for $I < 1$. For this reason, and for the fact that the M-dependence is trivially obtained through a Clebsch-Gordan coefficient, *The Quadrupole Moment*, Q, for a nucleus is uniquely defined via a state for which $M = I$ as

$$Q = \sqrt{\frac{16\pi}{5}} \langle IM = I|\hat{Q}^{20}|IM = I\rangle \,. \tag{4.5}$$

The prefactor is there to make Q equal to the zz-component of the quadrupole moment tensor.

The quadrupole moment Q is referred to as the *spectroscopic* quadrupole moment which is an observable in the laboratory system. It is to be distinguished from the quadrupole moment in the internal system which is, however, not an observable.

4.2 The Reduced Transition Rate

Classically, a non-spherical and charged rotating body will emit electromagnetic radiation in a continuous way. This process will gradually reduce the rotation because of the energy loss into radiation.

In the quantum regime this picture is replaced by a discontinuous process. The energy emitted is in form of photons which allow for the system to transfer between eigenstates of the nuclear Hamiltonian; states with specific energy and angular momentum. Also, the continuous flow of radiation becomes a probability process; either a photon is emitted or it is not. This probability is associated with a lifetime of the state.

The transitions can be classified into electromagnetic multipoles mediated by the multipole operators $\hat{Q}^{\lambda\mu}$. For a given multipole the emitted photon

carries a total angular momentum λ (in units of $\hbar$) with the projection μ onto the laboratory z-axis.

The transition rate Γ, which corresponds to the lifetime $\tau = \hbar/\Gamma$, from an initial nuclear eigenstate, $|I_i M_i\rangle$, to a final one, $|I_f M_f\rangle$, for an electrical multipole of order λ is given by [24], in SI-units,

$$\Gamma_{fi}^{\lambda\mu} = \frac{2}{\hbar\varepsilon_0}\frac{\lambda+1}{\lambda[(2\lambda+1)!!]^2}\left(\frac{E_\gamma}{\hbar c}\right)^{2\lambda+1} |\langle I_f M_f|\hat{Q}^{\lambda\mu}|I_i M_i\rangle|^2 \tag{4.6}$$

where E_γ is the energy of the emitted photon. This expression is derived from the interaction between the electromagnetic field and the nuclear charge distribution with "Fermi's golden rule" up to first order in perturbation theory.

Due to the fact that quadrupole deformations are the dominant degrees of freedom for the nuclear shape, the quadrupole mode is the strongest one for the radiation. These are the $E2$-transitions and are the ones which are considered in this work.

Often one does not want to distinguish between different M-values; neither for final nor initial states. Therefore one averages over initial M_i (assuming an ensemble of initial states evenly distributed over all possible M-values) and sum over final M_f (the final M-value is not important). This type of rate is therefore given by, for $\lambda = 2$,

$$\begin{aligned}
\Gamma_{fi}^{\lambda=2} &= \frac{1}{2I_i+1}\sum_{M_i=-I_i}^{I_i}\sum_{M_f=-I_f}^{I_f}\sum_{\mu=-2}^{2}\Gamma_{fi}^{2\mu} \\
&= \frac{1}{75\hbar\varepsilon_0}\left(\frac{E_\gamma}{\hbar c}\right)^5\frac{1}{2I_i+1}\sum_{M_i=-I_i}^{I_i}\sum_{M_f=-I_f}^{I_f}\sum_{\mu=-2}^{2}|\langle I_f M_f|\hat{Q}^{2\mu}|I_i M_i\rangle|^2 \\
&\equiv \frac{1}{75\hbar\varepsilon_0}\left(\frac{E_\gamma}{\hbar c}\right)^5 B(E2; I_i \to I_f)
\end{aligned} \tag{4.7}$$

where the *Reduced Transition Rate*, B, has been defined. All the information of the wave functions goes into the $B(E2)$-value. Therefore, when investigating the nuclear structure, this quantity is a better choice to study than the transition rate. Furthermore, the reduced transition rate does not contain the high E_γ-dependence of the transition rate and is therefore not sensitive to the level spacing of the states.

4.3 Formalism within The Model

In order to calculate the reduced transitions in a formally exact way, as described in Sec. 4.2, one needs angular momentum eigenstates. At the mean-field level, which breaks rotational symmetry, calculating the transitions inevitably contains assumptions and approximations.

In contrast, when angular momentum projection is performed, as in the model presented in this thesis, the transitions can be extracted in a natural and straightforward way. In addition, since the model allows for a large many-body basis, no effective charges are needed to be introduced which is a common feature in shell model calculations.

The model produces wave functions of the form (3.32). With these states, the matrix element in the expression of the reduced transition rate (4.7) can be expressed as

$$\begin{aligned}&\langle NZ, I'M', n'|\hat{Q}^{2\mu}|NZ, IM, n\rangle \\ &\qquad = \sum_{a'K'}\sum_{aK} h^{n'*}_{a'K'} h^{n}_{aK} \,\langle\phi_{a'}|\hat{P}^{I'\dagger}_{M'K'}\hat{Q}^{2\mu}\hat{P}^{I}_{MK}\hat{P}^{N}\hat{P}^{Z}|\phi_a\rangle\,.\end{aligned} \tag{4.8}$$

Here it has been used that $\hat{Q}^{2\mu}$ commutes with the particle number projection operators; however, it does not commute with the angular momentum operator. In Ref. [60] it is stated that

$$\begin{aligned}\hat{P}^{I'\dagger}_{M'K'}\hat{Q}^{2\mu}\hat{P}^{I}_{MK} &= \langle IM; 2\mu|I'M'\rangle \\ &\quad\times \sum_{\nu}\langle I, K'-\nu; 2\nu|I'K'\rangle\,\hat{Q}^{2\nu}\hat{P}^{I}_{K'-\nu,K}\end{aligned} \tag{4.9}$$

where the scalar products are Clebsch-Gordan coefficients and the sum goes over all ν for which the Clebsch-Gordan coefficient within the sum is non-zero. With this, the matrix element (4.8) becomes

$$\begin{aligned}&\langle NZ, I'M', n'|\hat{Q}^{2\mu}|NZ, IM, n\rangle \\ &\qquad = \langle IM; 2\mu|I'M'\rangle \sum_{a'K'}\sum_{aK} h^{n'*}_{a'K'} h^{n}_{aK} \\ &\qquad \times \sum_{\nu}\langle I, K'-\nu; 2\nu|I'K'\rangle\;\langle\phi_{a'}|\hat{Q}^{2\nu}\hat{P}^{I}_{K'-\nu,K}\hat{P}^{N}\hat{P}^{Z}|\phi_a\rangle\,.\end{aligned} \tag{4.10}$$

Note that the spectroscopic quadrupole moment Q (4.5) can be found from the matrix element (4.10). This is done by putting $I' = I$, $M' = M = I$, $n' = n$ and $\mu = 0$.

In the expression for the $B(E2)$-value, Eq. (4.7), the summations over M', M and μ only act on the first Clebsch-Gordan coefficient in the matrix element (4.10). Using orthogonality relations for the Clebsch-Gordan coefficients, the sum reduces to

$$\sum_{M=-I}^{I} \sum_{M'=-I'}^{I'} \sum_{\mu=-2}^{2} |\, \langle IM; 2\mu | I'M' \rangle \,|^2 = \sum_{M'=-I'}^{I'} 1 = 2I' + 1. \tag{4.11}$$

The final expression for the reduced transition rate in the model then is

$$\begin{aligned} &B(E2; I \to I') \\ &\quad = \frac{2I'+1}{2I+1} \left| \sum_{a'K'} \sum_{aK} h^{n'*}_{a'K'} h^{n}_{aK} \right. \\ &\quad \left. \times \sum_{\nu} \langle I, K' - \nu; 2\nu | I'K' \rangle \; \langle \phi_{a'} | \hat{Q}^{2\nu} \hat{P}^{I}_{K'-\nu,K} \hat{P}^{N} \hat{P}^{Z} | \phi_a \rangle \right|^2 . \end{aligned} \tag{4.12}$$

An explicit expression for the matrix element of the quadrupole operator within the basis of projected HFB-states, which appears in the expression (4.12), is given in App. C.2.

Chapter 5

Computations and Results

Using The Model to Investigate Nuclear Spectra, Rotational Bands, Backbending, Transitions and Quadrupole Moments

The best place to dig a very deep pit in which to catch a Heffalump,
is somewhere where a Heffalump already is,
only about a foot farther on or so.
— Winnie-the-Pooh

In this chapter a test case will be presented. The purpose is to demonstrate how a full sized calculation within the model is performed.

The different steps of the computer code behind the model will be outlined. A schematic picture for the structure of the code is shown in App. A. Input values and the following calculation times for the different parts are presented. The calculations make use of a partition of a *High Performance Computing Cluster* consisting of 18 nodes each with 20 cores. This implies that 360 computations can be made in parallel when possible and necessary.

Techniques for reducing the computational load will be described. The bottleneck for the model is the angular momentum projection within the GCM. Therefore, efforts of speeding up the process are focused on that part.

The results for the spectra and the electromagnetic transitions will be

presented together with comparisons to experiment. Physical interpretations of the results are discussed.

5.1 Computations for the Nucleus ^{48}Cr

The nucleus ^{48}Cr has been chosen as an example of the computations that are performed within the model. More results for other nuclei can be found in Papers III and IV.

As schematically shown in App. A, the code consists of two main blocks which are further subdivided into smaller boxes. The first block is at the mean-field level. Here all the single-particle quantities are generated within Nuclear-DFT. Results obtained from an EDF are mapped into the Effective Hamiltonian by adjusting the free parameter χ.

The second block reaches the beyond-mean-field level. It builds upon the Nuclear-DFT with the inclusions of the GCM, temperature and projections. The spectra and wave functions are obtained by solving the Hill-Wheeler equation. The results are further used to calculate electromagnetic transition rates.

5.2 Mean-Field – Single-Particle Quantities

The Nuclear-DFT calculations contain two parts. First, the spherical single-particle quantities. These are the single-particle spectra, $\{e_i\}$ and $\{a_i^\dagger\}$, which generates the single-particle basis and, within that basis, the matrix elements of the quadrupole operators: the modified, $\widetilde{Q}_{ij}^{2\mu}$, and the ordinary, $Q_{ij}^{2\mu}$. Second, χ is adjusted in such a way that the binding energy as a function of quadrupole deformation at the HF-level, $E^{\mathrm{HF}}(\beta)$, obtained with the Effective Hamiltonian reproduces the same quantity from an EDF as good as possible.

In this particular calculation, the EDF used is the Skyrme based parametrization SLy4 [33]. The single-particle quantities are calculated within an updated version of the code HOSPHE [62]. The basis consists of 12 spherical harmonic oscillator shells; a collection of 910 basis states. This size is chosen as large as possible while providing an acceptable calculation

time for the beyond-mean-field block of the code. The results from the calculation indicates that this basis is enough to produce reliable results.

In order to fix the free parameter χ, the energy $E^{\mathrm{HF}}(\beta)$ obtained from the Effective Hamiltonian, in the way described in Sec. 3.3, is compared with an EDF. The Nuclear-DFT calculation of $E^{\mathrm{HF}}(\beta)$ from an EDF is done for axial symmetry with the code HFBTHO [7]. Also in this code, in order to have a consistent comparison, the parametrization SLy4 and 12 harmonic oscillator shells are used.

The total calculation time at the mean-field level is basically free; in the order of 10 minutes.

5.3 Beyond-Mean-Field – Many-Body Quantities

With the Effective Hamiltonian fixed from Nuclear-DFT, it can be used in a straightforward way in the GCM together with projections.

5.3.1 The Many-Body Basis

The many-body basis to be used in the GCM consists of HFB-states with different constraints on β, γ, I_x, g_n and g_p as described in Sec. 3.4. The basis states are represented by the U- and V-matrices which define the quasiparticles in Eq. (2.7). These matrices are calculated from the HFB-equations (2.11).

For this calculation, the (β, γ)-plane is sampled with 300 states within $\beta \leq 0.5$ and $-30^\circ \leq \gamma \leq 150^\circ$. Only states below 12 MeV in excitation energy is kept; resulting in a basis size of 198 HFB-states.

The calculation of the 300 HFB-states is completed within five hours.

5.3.2 GCM and Projections

The most time-consuming part within the code is the calculations of the matrix elements in the many-body basis of projected HFB-states. Therefore, efforts have been made in order to reduce the computational cost of this part.

Reduction of the Space for the Angular Momentum Projection

The projection onto good angular momentum is especially time-consuming due to the simultaneous summation over the three Euler angles. Fortunately, restricting the HFB-states to have good parity and signature, the intervals of integration can be reduced; see Ref. [37]. Because of the symmetries of such a state, the full intervals of α, β and γ, see Eq. (2.18), can be mapped onto a smaller region. Here we have implemented the reduction of the region to be $\alpha \in [0, \pi/2]$, $\beta \in [0, \pi/2]$ and $\gamma \in [0, 2\pi]$; that is 1/8 of the full region. There is an additional possibility to cut the interval of γ into half; with the cost of introducing time reversed versions of the HFB-states. However, this has not been used in this work.

Truncation of Pairing Tails

The matrices which are appearing in the explicit expressions of the matrix elements, see for example Eq. (C.8), are all square matrices with a dimension equal to the number of states in the single-particle basis. In order to speed up the matrix multiplications, a truncation of the matrices are preferable. This can be achieved within the so called *canonical basis* which is reached through the Bloch-Messiah transformation [24]. In this basis the density matrix becomes diagonal; $\rho_{ij} = \rho_i \delta_{ij}$. First, the states are sorting such that the ρ_i's become in descending order. Then, a truncation is performed by setting $\rho_i = 0$ for $i > n$ where n is chosen such that

$$\sum_i \rho_i - \sum_i^n \rho_i < 0.01. \tag{5.1}$$

Hence, a truncation in the canonical basis corresponds to eliminating long pairing tales and numerical noise.

After the truncation, and with both states expressed in their own canonical basis, the transition densities, Eq.(C.4,C.5,C.6), get the structure

$$\rho^{ab} = \begin{pmatrix} \rho_{11}^{ab} & 0 \\ 0 & 0 \end{pmatrix}, \quad \kappa^{ab} = \begin{pmatrix} \kappa_{11}^{ab} & \kappa_{12}^{ab} \\ 0 & 0 \end{pmatrix}, \quad \kappa^{ba*} = \begin{pmatrix} \kappa_{11}^{ba*} & 0 \\ \kappa_{21}^{ba*} & 0 \end{pmatrix} \tag{5.2}$$

where the (1,1)-block is of the size $n \times n$. By expressing all matrices in the same 2×2-structure, the matrix multiplications can be evaluated with smaller matrices. See Paper III for more details.

Hermitian Matrices

As a last symmetry to use, both the Hamiltonian matrix and the overlap matrix are Hermitian. Therefore only the upper triangle, including the diagonal, of the matrices needs to be explicitly calculated.

However, the quadrupole operator, which are used for the calculations of transitions, does couple states with different angular momenta. In that case there is no obvious relation between the upper and lower triangles. In App. D such a relation is derived.

Input Values

This particular calculation uses 10 points in the particle number projections for both nucleon species and (9, 18, 36) points for the Euler angles which is equivalent with (36, 36, 36) points in the full region. Since the number projections for the two nucleon species are performed independent of each other, the total number of points for the projections becomes $(10 + 10) \times 9 \times 18 \times 36 = 116,640$.

The matrix elements in the many-body basis are distributed among the 18 nodes and for each element the angular momentum projection is distributed over 20 cores. With 198 states in the many-body basis, the total calculation time for all the $198(198 + 1)/2 = 19,701$ matrix elements is about 100 hours.

5.3.3 The Hill-Wheeler Equation

The Hill-Wheeler equation is solved once for every projected angular momentum. Since $0 \leq K \leq I$, the basis size is $N_\phi \times (I + 1)$ where N_ϕ is the number of HFB-states in the many-body basis.

For ^{48}Cr the maximum spin to be projected out is $I = 16$; in order to follow the yrast band up to termination. Hence, the largest matrices appearing in the Hill-Wheeler equation is of the size $198 \times (16 + 1) = 3,366$.

The calculation time to solve for H_{eff} with $I = 16$ is about 24 hours.

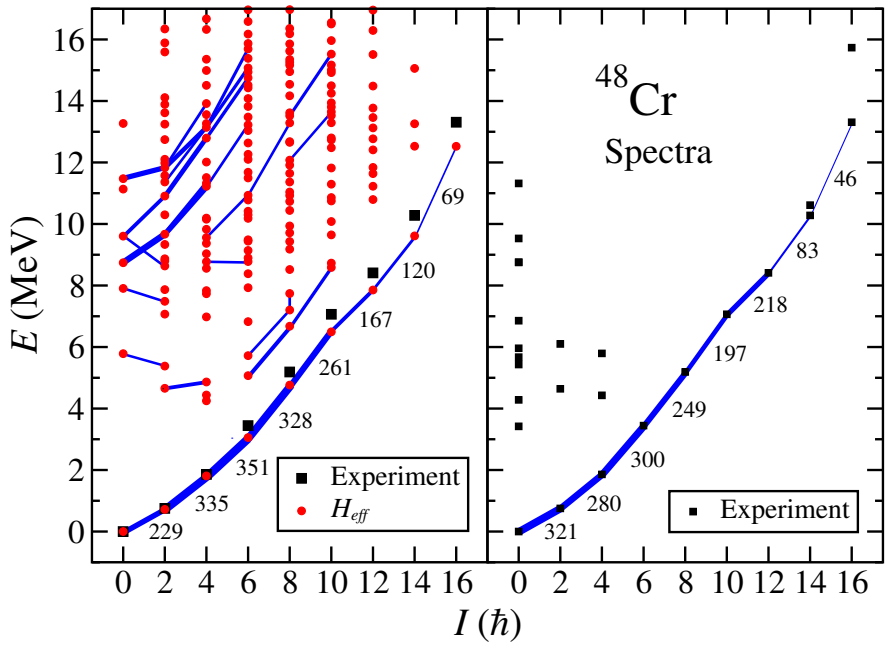

Figure 5.1: Spectra and $E2$-transitions for ^{48}Cr. Results from the model are to the left and from experiment to the right. Also, the experimental values for the yrast band are shown together with theory for easier comparison. The $B(E2)$-values are indicated by the thickness of the lines and are explicitly given in units of $e^2\text{fm}^4$ for the yrast band.

5.4 Results

The spectra for ^{48}Cr, both from the model and from experiment, together with the strongest $E2$-transitions are shown in Fig. 5.1. The experimental values are taken from Ref. [3]. The $B(E2)$-values are calculated between all pairs of states that differ with either two or zero units of angular momentum. However, only transitions over 10 Weisskopf units in strength are plotted in the spectra. A Weisskopf unit is the expected $B(E2)$-value if the transition is of a single-particle nature; about 10 $e^2\text{fm}^4$ for ^{48}Cr.

The results from the model show the characteristics of a rigid rotor. That is, for the yrast band, the energy grows approximately quadratic with angular momentum. At $I = 10$ a backbending occur. The backbending from the model is compared with experiment in figure 5.2; in which the released γ-energies within the yrast band are displayed. It can bee seen that, both in the model and in experiment, the backbending occurs at the same angular momentum and has the same magnitude. However, the

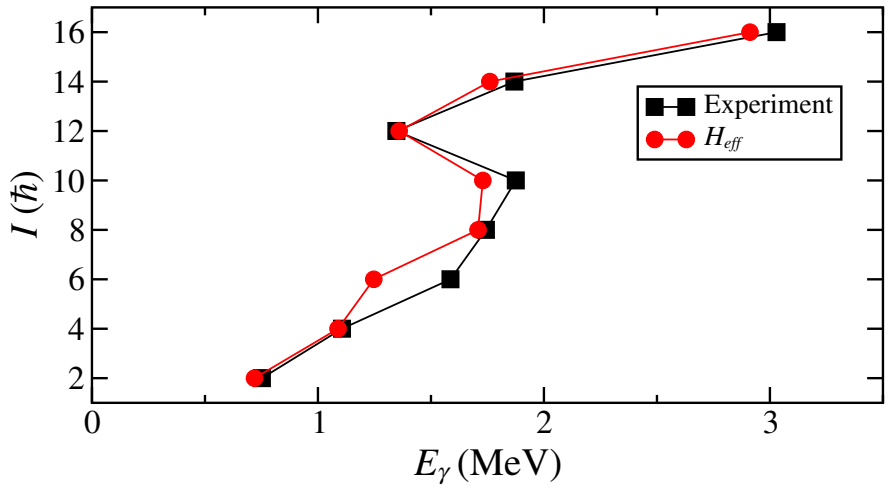

Figure 5.2: Released γ-energies for the transitions $I + 2 \rightarrow I$ within the yrast band. The backbending at $I = 10$ indicates a change in the internal structure.

γ-energies are consistently lower for the other angular momenta.

Also, in the spectrum from H_{eff} in Fig. 5.1, one can notice the transitions at high excitation energies. In specific, between 10 MeV and 16 MeV at $I = [2, 6]$ the cluster of transitions show the characteristics of the so called *Rotational Damping* [63]. A rotational band can be viewed as originating from a rotating mean-field state. Close to the yrast band this picture works well. However, high above the yrast band, where the level density is large, the mean-field states are expected to be highly mixed. As a consequence of that, the transitions do not form pure bands. Instead, an initial state with angular momentum I_i can have strong transitions into several states with $I = I_i - 2$; all corresponding to slightly different γ-energies. The same is true for the subsequent transitions. Thus, an ensemble of nuclei, all populating the same initial state, will form a cascade; a damped band. Those damped bands are a challenge to observe experimentally. The γ-energies from a given initial state become broaden and hard to distinguish from the background. In a theoretical spectrum the damped bands show up as a cluster of bands close to each other as in Fig. 5.1.

The evolution of the internal structure of ^{48}Cr with increasing angular momentum, up to its terminating state, has been investigated in Ref. [64] within the *Cranked Nilsson-Strutinsky* (CNS) model. One conclusion in this reference is that the intrinsic deformation starts from an axially symmetric prolate shape at $I = 0$, evolves over triaxial shapes and ends up in

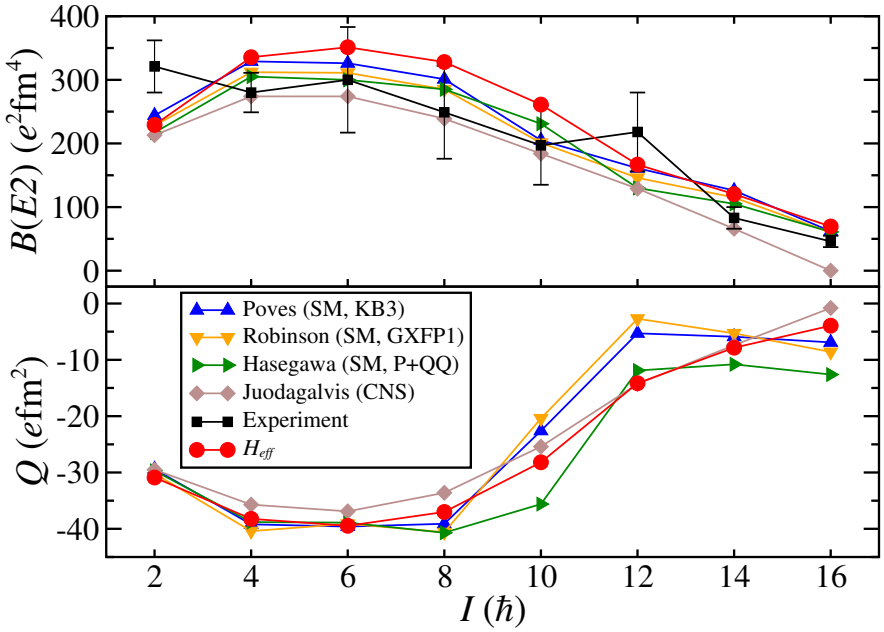

Figure 5.3: The reduced transitions $B(E2; I \rightarrow I-2)$ and spectroscopic quadrupole moments Q for the yrast band in ^{48}Cr. The abbreviations for the SM-calculations represent different types of interactions. No experimental data has been found for Q.

a slightly oblate shape for the terminating state at $I = 16$.

Comparisons for the reduced transition rates and for the spectroscopic quadrupole moments between the model and CNS are shown in Fig. 5.3. In addition, three shell model (SM) calculations for three different interactions within the full fp-space from Ref. [65, 66, 67] are included.

The results from the model are in agreement with previous calculations; both for CNS and SM. The behaviors for $B(E2)$ and for Q are similar to that of a rigid rotor up to $I = 6$. For higher angular momenta, the $B(E2)$-value is approaching zero; showing that these states are of a single-particle nature rather than of a mixed collective nature. Also, Q indicates a drastic change in the nuclear shape around the backbending and that the nucleus approaching a spherical shape at the terminating state.

The intrinsic nuclear deformation can be visualized directly from the collective wave function which the model gives as output. This is described in Paper 5.

Chapter 6

Outlook

Improve upon The Model
and Tackling Scientific Questions

Rivers know this: There is no hurry.
We shall get there some day.
— Winnie-the-Pooh

The simplicity of the Effective Hamiltonian presented in this thesis allows for reasonable calculation times; even for Super-Heavy Nuclei. At the same time, it seems like the Effective Hamiltonian captures enough physics in order to give accurate results for the spectrum; features as rotational bands, backbending and transition rates are well described. Also, due to the projections onto good quantum numbers, all observables are given in the laboratory system.

Theoretical Uncertainties

To quantify the confidence in predictions made by the model one can incorporate *theoretical uncertainties*. It would be interesting to know how the uncertainties in the parameters of the underlying EDF propagate to the outputs from the model. For example, uncertainties in the parameters of UNEDF1 are available [35]; both the standard deviations and the

correlation between them all. An estimate of the uncertainty in the final spectrum could be to first investigate how the fitting parameter χ in the Effective Hamiltonian varies within the uncertainties of the parameters. Then see, within the same many-body basis, how the energies are affected by the change in χ. This approach would avoid the process of recalculating the many-body matrix element for every set of values for the parameters which is the most time-consuming part in the model.

Octupole Interaction and $\mathcal{CP}$-violation

It is under development to include an *octupole interaction* in the Effective Hamiltonian. In the same way as for the quadrupole interaction, it comes with an adjustable strength. This strength is fitted to Nuclear-DFT-results in the octupole degree of freedom. The cost for introducing an octupole interaction is, with everything else the same, an increase of the calculation time with roughly a factor of two.

In addition to the improvement that comes when adding more degrees of freedom for the nucleus to explore, the octupole extension makes it possible for the model to be a tool for the investigation of *the baryon asymmetry* in the Universe: Why is there more matter than anti-matter?

One of the Sakharov conditions [68] for generating baryons is the $\mathcal{CP}$-violation. That is, Nature does not respect the combined symmetries of charge conjugation and parity. Indeed, $\mathcal{CP}$-violation is built into the Standard Model of Particle Physics. However, it seems that the violation is too small in order to explain the observed asymmetry between matter and anti-matter. Thus, this indicates physics beyond the Standard Model which can contribute to the $\mathcal{CP}$-violation.

A measurable quantity that is a direct proof of $\mathcal{CP}$-violation is the static electric dipole moment for a system in its ground state [69]. No such moment has not yet been found. But Several ongoing experimental efforts are conducted on different systems at different scales. Such as nucleons, light nuclei, atoms and molecules [70].

Specifically, the electric dipole moment of an atom is induced by the *Schiff moment* of the nucleus [69]. Therefore, having accurate predictions of the Schiff moment for a large range of nuclei would hint to the nuclear isotope with the largest probability for a positive measurement.

It is known that the Schiff moment is enlarged in heavy nuclei which are both quadrupole and octupole deformed in the intrinsic system. However, in the intrinsic system the Schiff moment can be trivially non-zero without $\mathcal{CP}$-violation because of symmetry breaking. Hence, it is important to perform the calculations in the laboratory system.

Since the Schiff moment is a ground state property of heavy and deformed nuclei, and inevitably needs to be calculated in the laboratory system, it is well suited for the model presented in this thesis. Therefore, with the inclusion of octupole deformation, the model could indeed be a tool for the theoretical search for nuclei with large Schiff moments.

Reactions

An area in which the model will be applied is *nuclear reactions*. See the Papers 1 and 2 for the first steps in that direction. Indeed, nuclear reactions are the main tool to experimentally explore features of the nuclear structure and to investigate the nuclear interaction. Furthermore, in order to interpret the experimental results from new facilities studying short lived nuclei through radio active ion beams a reliable scattering theory is needed.

An example of a fundamental question to be answered within nuclear reactions is the *nucleosynthesis* of elements heavier than iron in the Universe. The most probable mechanism of the production of heavy elements is through neutron capture. Preferably through the rapid neutron capture; the so called r-process. In order for a nucleus to accumulate neutrons, an enormous high flux of neutrons is needed. The most likely sites where this can happen are in supernovae and at neutron star mergers. Such extreme conditions are far beyond what current experiments can reach. However, there are astronomical observations which indicate that elements with $A > 260$ are produced through the r-process; then they undergo fission and β-decays into elements between iron and uranium in the periodic table [71]. But the reaction paths to the production of heavy elements are not well understood and therefore a reliable theoretical model for nuclear reactions is preferable.

A main tool for the theoretical study of reactions for heavy nuclei is the *Optical Potential*. This potential is for reactions what the mean-field is for nuclear structure; simplifying the complicated many-body system into an

approximate one-body potential. The optical potential is often constructed in a phenomenological way. However, it is preferable to derive the potential from microscopic interactions. See, for example, Ref. [72, 73] and further references therein for an overview of the importance of having a microscopic and united description of nuclear reactions and nuclear structure.

It is under development to use the nuclear spectrum from this model to construct the Green's function from which the optical potential can be derived. The model has the advantage to include deformation in an explicit way through the quadrupole interaction and at the same time be simple enough in order to be applied on Super-Heavy Nuclei.

References

[1] N. Bohr, Nature **112**, 29 (1923).

[2] Y. T. Oganessian and V. K. Utyonkov, Nucl. Phys. A **944**, 62 (2015).

[3] Evaluated nuclear structure data file, 2021, `http://www.nndc.bnl.gov`

[4] A. Sobiczewski, F. A. Gareev and B. N. Kalinkin, Phys. Lett. **22**, 500 (1966).

[5] S.-G. Nilsson, C. F. Tsang, A. Sobiczewski, Z. Szymański, S. Wycech, C. Gustafson, I.-L. Lamm, P. Möller and B. Nilsson, Nucl. Phys. A **131**, 1 (1969).

[6] P.-H. Heenen, J. Skalski, A. Staszczak and D. Vretenar, Nucl. Phys. A **944**, 415 (2015).

[7] M. V. Stoitsov, N. Schunck, M. Kortelainen, N. Michel, H. Nam, E. Olsen, J. Sarich and S. Wild, Comput. Phys. Commun. **184**, 1592 (2013).

[8] D. E. Ward, B. G. Carlsson and S. Åberg, Phys. Rev. C **92**, 014314 (2015).

[9] B. G. Carlsson and I. Ragnarsson, Phys. Rev. C **74**, 044310 (2006).

[10] G. Scamps, S. Goriely, E. Olsen, M. Bender and W. Ryssens, Eur. Phys. J. A **57**, 333 (2021).

[11] C. C. Chang, A. N. Nicholson, E. Rinaldi, E. Berkowitz, N. Garron, D. A. Brantley, H. Monge-Camacho, C. J. Monahan, C. Bouchard, M. A. Clark, B. Joó, T. Kurth, K. Orginos, P. Vranas and A. Walker-Loud, Nature **558**, 91 (2018).

[12] Y.-B. Yang, J. Liang, Y.-J. Bi, Y. Chen, T. Draper, K.-F. Liu and Z. Liu, Phys. Rev. Lett. **121**, 21 (2018).

[13] C. Drischler, W. Haxton, K. McElvain, E. Mereghetti, A. Nicholson, P. Vranas and A. Walker-Loud, Prog. Part. Nucl. Phys. **121**, 103888 (2021).

[14] C. Weizsäcker, Zeitschrift für Physik A Hadrons and Nuclei **96**, 431 (1935).

[15] H. A. Bethe and R. F. Bacher, Rev. Mod. Phys. **8**, 82 (1936).

[16] A. Bohr, Det Kongelige Danske Videnskabernes Selskab. Matematisk-fysiske Meddelelser **26**, 14 (1952).

[17] M. Goeppert Mayer, Phys. Rev. **78**, 16 (1950).

[18] M. Goeppert Mayer, Phys. Rev. **78**, 22 (1950).

[19] M. Goeppert Mayer and J. H. D. Jensen, *Elementary Theory of Nuclear Shell Structure* (Wiley, New York, 1955).

[20] R. D. Woods and D. S. Saxon, Phys. Rev. **95**, 577 (1954).

[21] S.-G. Nilsson, Det Kongelige Danske Videnskabernes Selskab. Matematisk-fysiske Meddelelser **29**, 16 (1955).

[22] E. Caurier, G. Martínez-Pinedo, F. Nowacki, A. Poves and A. P. Zuker, Rev. Mod. Phys. **77**, 427 (2005).

[23] D. C. Zheng, B. R. Barrett, L. Jaqua, J. P. Vary and R. J. McCarthy, Phys. Rev. C **48**, 1083 (1993).

[24] P. Ring and P. Schuck, *The Nuclear Many-Body Problem* (Springer-Verlag, New York, 1980).

[25] J. Dobaczewski and W. Nazarewicz, Hartree–Fock–Bogoliubov Solution of the Pairing Hamiltonian in Finite Nuclei, In R. A. Broglia and V. Zelevinsky (Eds.), *Fifty Years of Nuclear BCS: Pairing in Finite Systems* (World Scientific, Singapore, 2013), 40–60.

[26] D. R. Inglis, Phys. Rev. **96**, 1059 (1954).

[27] P. Hohenberg and W. Kohn, Phys. Rev. **136**, B864 (1964).

[28] J. Engel, Phys. Rev. C **75**, 014306 (2007).

[29] T. H. R. Skyrme, Nucl. Phys. **9**, 615 (1958).

[30] E. Chabanat, P. Bonche, P. Haensel, J. Meyer and R. Schaeffer, Nucl. Phys. A **627**, 710 (1997).

[31] D. Vautherin and D. M. Brink, Phys. Rev. C **5**, 626 (1972).

[32] M. Bender, P.-H. Heenen and P.-G. Reinhard, Rev. Mod. Phys. **75**, 121 (2003).

[33] E. Chabanat, P. Bonche, P. Haensel, J. Meyer and R. Schaeffer, Nucl. Phys. A **635**, 231 (1998).

[34] M. Beiner, H. Flocard, Nguyen Van Giai and P. Quentin, Nucl. Phys. A **238**, 29 (1975).

[35] M. Kortelainen, J. McDonnell, W. Nazarewicz, P.-G. Reinhard, J. Sarich, N. Schunck, M. V. Stoitsov and S. M. Wild, Phys. Rev. C **85**, 024304 (2012).

[36] J. Bartel, P. Quentin, M. Brack, C. Guet and H.-B. Håkansson, Nucl. Phys. A **386**, 79 (1982).

[37] B. Bally and M. Bender, Phys. Rev. C **103**, 024315 (2021).

[38] D. L. Hill and J. A. Wheeler, Phys. Rev. **89**, 1102 (1953).

[39] B. G. Carlsson, J. Toivanen and U. von Barth, Phys. Rev. C **87**, 054303 (2013).

[40] S. Geltman, J. At., Mol., Opt. Phys. **2011**, 573179 (2011).

[41] R. Balian and E. Brezin, Il Nuovo Cimento **64**, 37 (1969).

[42] D. Lacroix, T. Duguet and M. Bender, Phys. Rev. C **79**, 044318 (2009).

[43] F. Dönau, Phys. Rev. C **58**, 872 (1998).

[44] M. Waroquier, J. Ryckebusch, J. Moreau, K. Heyde, N. Blasi, S. Y. van der Werf and G. Wenes, Phys. Rep. **148**, 249 (1987).

[45] T. Duguet and P. Bonche, Phys. Rev. C **67**, 054308 (2003).

[46] W. Satuła and J. Dobaczewski, Phys. Rev. C **90**, 054303 (2014).

[47] J. P. Elliott, Proceedings of the Royal Society of London. Series A, Mathematical and Physical Sciences **245**, 562 (1958).

[48] S. T. Belyaev, Det Kongelige Danske Videnskabernes Selskab. Matematisk-fysiske Meddelelser **31**, 1 (1959).

[49] M. Baranger and K. Kumar, Nucl. Phys. **62**, 113 (1965).

[50] M. Baranger and K. Kumar, Nucl. Phys. A, **110**, 490 (1968).

[51] D. R. Bes and R. A. Sorensen, *The Pairing-Plus-Quadrupole Model* (Springer, New York, 1969), 129–222. .

[52] K. Hebeler, V. Durant, J. Hoppe, M. Heinz, A. Schwenk, J. Simonis and A. Tichai, Phys. Rev. C **107**, 024310 (2023).

[53] K. Kumar and B. Sørensen, Nucl. Phys. A **146**, 1 (1970).

[54] I. Ragnarsson and S.-G. Nilsson, *Shapes and Shells in Nuclear Structure* (Cambridge University Press, Cambridge, 1995).

[55] S Cwiok, J Dudek, W Nazarewicz, J Skalski and T Werner, Comput. Phys. Commun. **46**, 379 (1987).

[56] P. André, Master's degree, Lund University (2019).

[57] A. Tichai, R. Schutski, G. E. Scuseria and T. Duguet, Phys. Rev. C **99**, 034320 (2019).

[58] H. Olofsson, R. Bengtsson, and P. Möller, Nucl. Phys. A **784**, 104 (2007).

[59] R. Bengtsson and S. Åberg, Phys. Lett. B **172**, 277 (1986).

[60] K. Enami, K. Tanabe and N. Yoshinaga, Phys. Rev. C **59**, 135 (1999).

[61] B. G. Carlsson and J. Rotureau, Phys. Rev. Lett. **126**, 172501 (2021).

[62] B. G. Carlsson, J. Dobaczewski, J. Toivanen and P. Veselý, Comput. Phys. Commun. **181**, 1641 (2010).

[63] B. Lauritzen, T. Døssing and R. A. Broglia, Nucl. Phys. A **457**, 61 (1986).

[64] A. Juodagalvis, I. Ragnarsson and S. Åberg, Phys. Lett. B **477**, 66 (2000).

[65] A Poves, J. Phys. G: Nucl. Part. Phys. **25**, 589 (1999).

[66] S. J. Q. Robinson, T. Hoang, L. Zamick, A. Escuderos and Y. Y. Sharon, Phys. Rev. C **89**, 014316 (2014).

[67] M. Hasegawa, K. Kaneko and S. Tazaki, Nucl. Phys. A **674**, 411 (2000).

[68] A. D. Sakharov, Sov. Phys. Usp. **34**, 392 (1991).

[69] N. Auerbach and V. Zelevinsky, J. Phys. G: Nucl. Part. Phys. **35**, 093101 (2008).

[70] T. E. Chupp, P. Fierlinger, M. J. Ramsey-Musolf and J. T. Singh, Rev. Mod. Phys. **91**, 015001 (2019).

[71] I. U. Roederer, N. Vassh, E. M. Holmbeck, M. R. Mumpower, R. Surman, J. J. Cowan, T. C. Beers, R. Ezzeddine, A. Frebel, T. T. Hansen, V. M. Placco and C. M. Sakari, Science **382**, 1177 (2023).

[72] C. W. Johnson, K. D. Launey, *et.al*, J. Phys. G: Nucl. Part. Phys. **47**, 123001 (2020).

[73] C. Hebborn, F. M. Nunes, G. Potel, W. H. Dickhoff, J. W. Holt, *et.al*, J. Phys. G: Nucl. Part. Phys. **50**, 060501 (2023).

[74] Z.-C. Gao, Q.-L. Hu and Y.S. Chen, Phys. Lett. B **732**, 360 (2014).

Appendix A

Structure of Computer Code

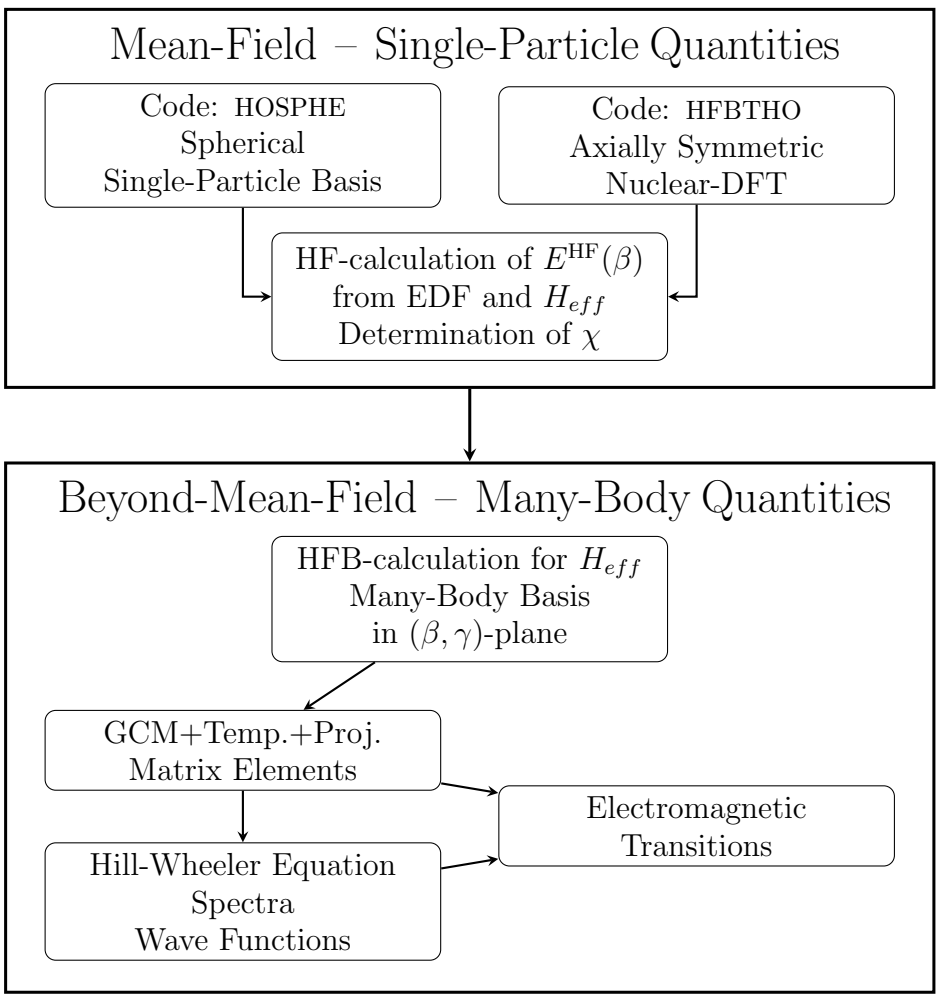

Appendix B

Discretization of Projection Operators

Particle Number Projection Operator

The integral of the particle number projection operator (2.17) can be discretized into M intervals as

$$\hat{P}^N \approx \frac{1}{\pi} \sum_{m=1}^{M} e^{i(\hat{N}-N)m\Delta\theta} \Delta\theta \tag{B.1}$$

where $\Delta\theta = \pi/M$. With $\theta = \theta(m) \equiv m\Delta\theta$, which has an implicit dependence on m, the projection operator can be expressed as

$$\hat{P}^N \approx \frac{1}{M} \sum_{\theta} e^{-iN\theta} e^{i\hat{N}\theta} \equiv \sum_{\theta} w^N(\theta) e^{i\hat{N}\theta} \tag{B.2}$$

where the weight $w^N(\theta)$ has been defined.

Angular Momentum Projection Operator

For the angular momentum projection operator (2.18), the integrals over the Euler angles (α, β, γ) can be discretized into (A, B, C) intervals. Hence,

$$\hat{P}^I_{MK} \approx \frac{2I+1}{8\pi^2} \sum_{a=1}^{A} \Delta\alpha \sum_{b=1}^{B} \Delta\beta \sin(\beta) \sum_{c=1}^{C} \Delta\gamma D^{I*}_{MK}(\Omega) \hat{R}(\Omega) \tag{B.3}$$

where $\Delta\alpha = 2\pi/A$, $\Delta\beta = \pi/B$, $\Delta\gamma = 2\pi/C$ and $\Omega \equiv (\alpha, \beta, \gamma) \equiv (a\Delta\alpha, b\Delta\beta, c\Delta\gamma)$ which has an implicit dependence on a, b and c. With that, the angular momentum projection operator can be written

$$\begin{aligned} \hat{P}^I_{MK} &\approx \frac{2I+1}{8\pi^2} \frac{4\pi^3}{ABC} \sum_{\Omega} \sin(\beta) D^{I*}_{MK}(\Omega) \hat{R}(\Omega) \\ &\equiv \sum_{\Omega} w^I_{MK}(\Omega) \hat{R}(\Omega) \end{aligned} \tag{B.4}$$

where the weight $w^I_{MK}(\Omega)$ has been defined.

Appendix C

Matrix Elements in the Many-Body Basis

C.1 The Effective Hamiltonian

With the discretization of the projection operators, described in App. B, the matrix elements of the Effective Hamiltonian (3.30) are given by

$$H_{a'K',aK} = \sum_{\Omega} \sum_{\theta_n \theta_p} w^I_{K'K}(\Omega) w^N(\theta_n) w^Z(\theta_p) \times \langle \phi_{a'} | H_{eff} \hat{R}(\Omega) e^{i\hat{N}\theta_n} e^{i\hat{Z}\theta_p} | \phi_a \rangle \,. \tag{C.1}$$

Define a rotated HFB-state as $\hat{R}(\Omega) e^{i\hat{N}\theta_n} e^{i\hat{Z}\theta_p} |\phi_a\rangle \equiv |\phi_b\rangle$ which depends implicit on θ_n, θ_p and Ω. The U- and V-matrices which define the quasi-particles, see Eq. (2.7), associated with the rotated state, (U_b, V_b), can be obtained from the matrices associated with the unrotated state, (U_a, V_a). According to Ref. [74], and from the fact that the total rotation is a unitary transformation, the relations are

$$U_b = \mathbb{R} U_a, \qquad V_b = \mathbb{R}^* V_a \tag{C.2}$$

where $\mathbb{R}$ is the matrix for the total rotation. Its elements are given by

$$\mathbb{R}_{kl} = \langle k | \hat{R}(\Omega) e^{i\hat{N}\theta_n} e^{i\hat{Z}\theta_p} | l \rangle = D^{j_l}_{m_k m_l} \delta_{j_k j_l} \left(e^{i\theta_n} \delta_{\tau_l n} + e^{i\theta_p} \delta_{\tau_l p} \right) \delta_{\tau_k \tau_l} \tag{C.3}$$

where D^j is the Wigner D-matrix for angular momentum j.

For each point of the discretized projections, a matrix element of the form $\langle\phi_a|H_{eff}|\phi_b\rangle$, where $|\phi_b\rangle$ is the rotated state, has to be calculated. The notation becomes simplified by introducing the transition densities [24]

$$\rho_{ij}^{ab} \equiv \frac{\langle\phi_a|a_j^\dagger a_i|\phi_b\rangle}{\langle\phi_a|\phi_b\rangle} = V_b^* \mathbb{U}^{-1} V_a^T, \tag{C.4}$$

$$\kappa_{ij}^{ab} \equiv \frac{\langle\phi_a|a_j a_i|\phi_b\rangle}{\langle\phi_a|\phi_b\rangle} = V_b^* \mathbb{U}^{-1} U_a^T, \tag{C.5}$$

$$\kappa_{ij}^{ba*} \equiv \frac{\langle\phi_a|a_i^\dagger a_j^\dagger|\phi_b\rangle}{\langle\phi_a|\phi_b\rangle} = -U_b^* \mathbb{U}^{-1} V_a^T \tag{C.6}$$

with

$$\mathbb{U} \equiv \left(U_a^T U_b^* + V_a^T V_b^*\right). \tag{C.7}$$

In Ref. [24] a formula for the matrix elements of a general two-body Hamiltonian in a basis of HFB-states is given. Using this formula for the Effective Hamiltonian (3.1), which contains the spherical single-particle potential (3.2), the modified quadrupole interaction (3.13) and the pairing interaction (3.16), one can derive that

$$\begin{aligned}
\frac{\langle\phi_a|H_{eff}|\phi_b\rangle}{\langle\phi_a|\phi_b\rangle} = & \sum_i e_i \rho_{ii} \\
& - \frac{1}{2}\chi \sum_{\mu=-2}^{2} \left[\mathrm{Tr}\left(\rho\widetilde{Q}^{2\mu\dagger}\right)\mathrm{Tr}\left(\rho\widetilde{Q}^{2\mu}\right) - \mathrm{Tr}\left(\rho\widetilde{Q}^{2\mu\dagger}\rho\widetilde{Q}^{2\mu}\right)\right] \\
& + \frac{1}{2}\sum_{q\in\{n,p\}} G^q \mathrm{Tr}\left(\rho P^q \rho^T P^q\right) \\
& + \frac{1}{2}\chi \sum_{\mu=-2}^{2} \mathrm{Tr}\left(\kappa^* \widetilde{Q}^{2\mu} \kappa \widetilde{Q}^{2\mu *}\right) \\
& - \frac{1}{4}\sum_{q\in\{n,p\}} G^q \mathrm{Tr}\left(\kappa^* P^q\right)\mathrm{Tr}\left(\kappa P^q\right)
\end{aligned} \tag{C.8}$$

where the super scripts ab and ba on the transition densities have been omitted in order to lighten the notation. When deriving this expression, the symmetries $P^{qT} = -P^q$ and $\kappa^T = -\kappa$ have been used.

C.2 The Quadrupole Operator

From Eq. (4.12) for the reduced transition rate, define the matrix elements of the quadrupole operator in the basis of projected HFB-states as

$$Q^{I'I}_{a'K',aK} = \sum_{\nu} \langle I, K' - \nu; 2\nu | I'K' \rangle \ \langle \phi_{a'} | \hat{Q}^{2\nu} \hat{P}^{I}_{K'-\nu,K} \hat{P}^{N} \hat{P}^{Z} | \phi_a \rangle \,. \tag{C.9}$$

With the discretized projection operators from App. B this becomes

$$\begin{aligned} Q^{I'I}_{a'K',aK} = & \sum_{\nu} \langle I, K' - \nu; 2\nu | I'K' \rangle \\ & \times \sum_{\Omega} \sum_{\theta_n \theta_p} w^{I}_{K'-\nu,K}(\Omega) w^{N}(\theta_n) w^{Z}(\theta_p) \\ & \times \ \langle \phi_{a'} | \hat{Q}^{2\nu} \hat{R}(\Omega) e^{i\hat{N}\theta_n} e^{i\hat{Z}\theta_p} | \phi_a \rangle \,. \end{aligned} \tag{C.10}$$

In the same way as for the Effective Hamiltonian in App. C.1, define the rotated state as $\hat{R}(\Omega) e^{i\hat{N}\theta_n} e^{i\hat{Z}\theta_p} \, |\phi_a\rangle \equiv |\phi_b\rangle$. For each point of the discretized projections a matrix element of the form $\langle \phi_a | \hat{Q}^{2\nu} | \phi_b \rangle$ has to be calculated. From expression (4.2) of the quadrupole operator, one can put up that

$$\begin{aligned} \langle \phi_a | \hat{Q}^{2\nu} | \phi_b \rangle &= \sum_{ij} Q^{2\nu}_{ij} \ \langle \phi_a | a^{\dagger}_i a_j | \phi_b \rangle \\ &= \langle \phi_a | \phi_b \rangle \sum_{ij} Q^{2\nu}_{ij} \rho^{ab}_{ji} = \langle \phi_a | \phi_b \rangle \, \mathrm{Tr}(Q^{2\nu} \rho^{ab}) \end{aligned} \tag{C.11}$$

where the definition of the transition density (C.4) has been used.

Appendix D

The Transpose of the Quadrupole Matrix

Here a relation for the transpose of the quadrupole matrix, as defined in Eq. (C.9), is derived. That is, knowing $Q^{I'I}_{a'K',aK}$, what is $Q^{I'I}_{aK,a'K'}$?

Comparing Eq. (4.10) and Eq. (4.8) together with the definition (C.9) of the quadrupole matrix, one can conclude that

$$Q^{I'I}_{a'K',aK} = \frac{\langle \phi_{a'} | \hat{P}^{I'\dagger}_{M'K'} \hat{Q}^{2\mu} \hat{P}^{I}_{MK} | \phi_a \rangle}{\langle IM; 2\mu | I'M' \rangle} \tag{D.1}$$

where the particle number projections are implicit in order to lighten the notation. However, from the definition (C.9), $Q^{I'I}_{aK,a'K'}$ does not depend on any of M, M' and μ. Hence, those can be put into any explicit values that do not make the Clebsch-Gordan coefficient to vanish identically. Therefore, put $\mu = 0$. Note that putting $M' = M = 0$ would exclude transitions for which $|I' - I| = 1$. Furthermore, from the conjugate symmetry of a scalar product of two states, one can obtain that

$$Q^{I'I}_{a'K',aK} = \frac{\langle \phi_a | \hat{P}^{I\dagger}_{MK} \hat{Q}^{20} \hat{P}^{I'}_{M'K'} | \phi_{a'} \rangle^*}{\langle IM; 20 | I'M' \rangle} = \frac{\langle I'M'; 20 | IM \rangle}{\langle IM; 20 | I'M' \rangle} Q^{II'*}_{aK,a'K'} \tag{D.2}$$

where it has been used that $\hat{Q}^{20}$ is hermitian and the Clebsch-Gordan coefficients are real. Explicit, this can be written

$$Q^{I'I}_{a'K',aK} = (-1)^{I'-I} \sqrt{\frac{2I+1}{2I'+1}} Q^{II'*}_{aK,a'K'} \tag{D.3}$$

which is the desired relation.

Part II

Scientific Publications

Author's Contributions and The Papers Reproduced

Author's Contributions

Paper I: Low-lying states in ^{219}Ra and ^{215}Rn: Sampling microsecond α-decaying nuclei

I performed the calculations that investigated the octupole deformation and α-decay rates of the nucleus ^{219}Ra. The results are presented in Fig. 7, Table IV and Table V. I wrote Sec. VI A and Sec. VI D. I participated in the interpretation of the spectrum for ^{219}Ra.

Paper II: Spectroscopy along Flerovium Decay Chains: Discovery of ^{280}Ds and an Excited State in ^{282}Cn

I contributed in the writing of the computer code that performs the calculations within the model presented in this thesis. This code was used to calculate the spectra for ^{282,284,286,288}Cn in Fig. 2(b).

Paper III: Nuclear spectra from low-energy interactions

I constructed the formalism for the electromagnetic moments and transition rates within the model and I wrote the corresponding computer code. I performed the calculations for ^{48,50,52}Cr and ^{24}Mg and produced the corresponding figures. I investigated how the spectrum of ^{24}Mg is affected by the inclusion of temperature. I wrote Sec. II G, App. B and the major part of Sec. III. Results. I made additional contributions to the contents and to the overall structure of the paper.

Paper IV: Beyond-Mean-Field with an Effective Hamiltonian Mapped from an Energy Density Functional

I extended the computer code to include odd numbered angular momentum states. I wrote the whole paper, performed all the calculations and produced all figures.

Svåra fakta om Atomkärnor

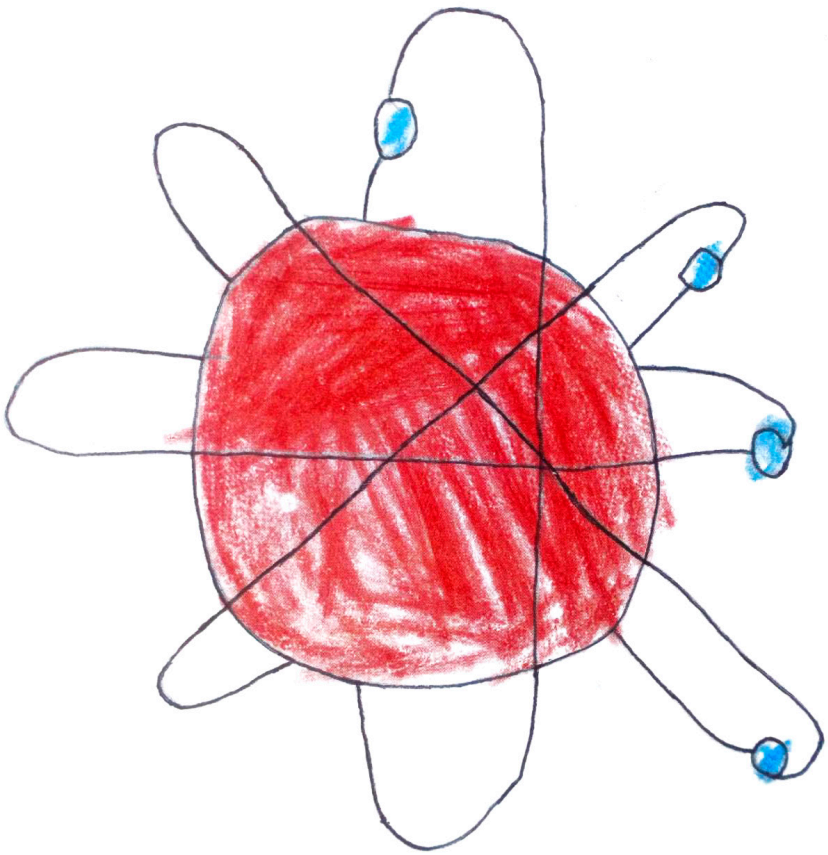

Printed by Media-Tryck, Lund 2024 NORDIC SWAN ECOLABEL 3041 0903

LUND UNIVERSITY

Division of Mathematical Physics
Department of Physics
Faculty of Engineering

ISBN 978-91-8104-135-4